Atmospheric CH_4 oxidation by Arctic permafrost and mineral cryosols as a function of water saturation and temperature

B. Stackhouse[1]; M.C.Y. Lau[1]; T. Vishnivetskaya[2], N. Burton; R. Wang; A. Southworth; L. Whyte[3]; T.C. Onstott[1]

[1]Department of Geosciences, Princeton University, NJ, USA

[2]The Center for Environmental Biotechnology, University of Tennessee, Knoxville, TN, USA

[3]Department of Natural Resource Sciences, McGill University, QC, Canada

N. Burton, R. Wang, and A. Southworth are not currently affiliated with research institutions but were at Princeton during the time of the research.

Corresponding author: T.C. Onstott

Mailing address: B79 Guyot Hall, Dept. of Geosciences, Princeton University, Washington Road, Princeton, NJ 08544

Email address: tullis@princeton.edu

Telephone: 609-258-7678

Fax: N/A

This is the author manuscript accepted for publication and has undergone full peer review but has not been through the copyediting, typesetting, pagination and proofreading process, which may lead to differences between this version and the Version of Record. Please cite this article as doi: 10.1111/gbi.12193

Article Type: Original Article

Atmospheric CH_4 oxidation by Arctic permafrost and mineral cryosols as a function of water saturation and temperature

Running Title: **Atmospheric CH_4 oxidation by Arctic mineral cryosols**

B. Stackhouse[1]; M.C.Y. Lau[1]; T. Vishnivetskaya[2], N. Burton[1]; R. Wang[1]; A. Southworth[1]; L. Whyte[3]; T.C. Onstott[1]

[1]Department of Geosciences, Princeton University, NJ, USA

[2]The Center for Environmental Biotechnology, University of Tennessee, Knoxville, TN, USA

[3]Department of Natural Resource Sciences, McGill University, QC, Canada

Keywords: methanotrophs, stable isotope labeling, microcosms

Abstract (200 words)

The response of methanotrophic bacteria capable of oxidizing atmospheric CH_4 to climate warming is poorly understood, especially for those present in Arctic mineral cryosols. The atmospheric CH_4 oxidation rates were measured in microcosms incubated at 4°C and 10°C along a 1 m depth profile and over a range of water saturation conditions for mineral cryosols containing Type I and Type II methanotrophs from Axel Heiberg Island (AHI), Nunavut, Canada. The cryosols exhibited net consumption of ~2 ppmv CH_4 under all conditions, including during anaerobic incubations. Methane oxidation rates increased with temperature and decreased

with increasing water saturation and depth, exhibiting the highest rates at 10°C and 33% saturation at 5 cm depth (260±60 pmol CH_4 gdw^{-1} d^{-1}). Extrapolation of the CH_4 oxidation rates to the field yields net CH_4 uptake fluxes ranging from 11 to 73 µmol CH_4 m^{-2} d^{-1}, which are comparable to field measurements. Stable isotope mass balance indicates ~50% of the oxidized CH_4 is incorporated into the biomass regardless of temperature or saturation. Future atmospheric CH_4 uptake rates at AHI with increasing temperatures will be determined by the interplay of increasing CH_4 oxidation rates versus water saturation and the depth to the water table during summer thaw.

Introduction

The response of terrestrial ecosystems, especially those located in the Arctic, to rapid global warming is the subject of much debate that centers on the impact of future greenhouse gas emissions and feedbacks (Lawrence et al., 2008; Allison et al., 2010; Graham et al., 2012). Arctic permafrost and overlying active layers contain approximately one third of the global soil organic carbon (SOC) stocks shallower than 3 meters (Schuur et al., 2008). These reserves will be particularly impacted by climate change as deepening of the seasonally thawed active layer reintroduces the previously sequestered permafrost SOC to the active carbon cycle (Rowlands et al., 2012). Based upon modeling experiments, Hayes et al. (2014) have estimated that Arctic warming from 1970 to 2006 has already exposed an additional 11.6 Pg of SOC to microbial degradation, and that this exposure has resulted in the net emission of 3.7 Pg of CO_2 and 0.03 Pg of CH_4. Not considered in their model are the impacts of slumps associated with permafrost degradation that create new hydrological conditions, such as thermokarst lakes or dry upland cryosols, throughout Arctic regions (Jorgenson et al., 2006; Osterkamp, 2007; Grosse et al., 2011). The expansion of thermokarst lakes and flooded cryosols in Siberian permafrost where Pleistocene-age SOC is undergoing rapid conversion to CH_4 under anaerobic conditions has been tied to increases in regional CH_4 emissions (Walter et al., 2006). Although atmospheric CH_4 concentrations at a global scale remained relatively stable at 1.78 ppmv from 1999 to 2006, they have increased from 2007 to 2010 to 1.8 ppmv (Dlugokencky et al., 2014). CH_4 has a global warming potential 75 times greater than that of CO_2 over a 20-year timescale (Shindell et al., 2009) and at 1.8 ppmv, atmospheric CH_4 accounts for ~18% of the greenhouse gas radiative forcing (Montzka et al., 2011). This recent upward trend in atmospheric CH_4 concentrations

appears to be caused by global meteorological factors and is not due to release from Arctic SOC stocks even though Arctic temperatures have been steadily increasing during this time period (Dlugokencky et al., 2014). This apparent paradox may stem from the fact that the majority of field research on Arctic CH_4 fluxes has been performed at sites in Siberia, Greenland, and Alaska where a high-SOC, CH_4–emitting active layer overlies permafrost that is slowly thawing (Table 1). Various other Arctic sites, however, have recently been found to be net sinks of atmospheric CH_4 (Whalen & Reeburgh, 1990, 1992; Adachi et al., 2006; Kolb, 2009; Bäckstrand et al., 2010; Liebner et al., 2011; Brummell et al., 2012, 2014; Allan et al., 2014; Emmerton et al., 2014; Lau et al., 2015; Stackhouse et al., 2015, See Table 1). With a few exceptions these sites are located in mineral cryosols that contain <50 kg SOC m^{-2} and which comprise 87% of permafrost-impacted regions (Hugelius et al., 2014). The ability of soils to oxidize CH_4 from the atmosphere has also been increasingly connected to the presence of high-affinity methanotrophic bacteria based upon detection of a specific pmoA marker gene (e.g. Upland Soil Cluster alpha) (Knief & Dunfield, 2005; Kolb, 2009; Degelmann et al., 2010; Martineau et al., 2014; Lau et al., 2015), even though these bacteria have not yet been isolated in the lab. Soils containing high-affinity methanotrophic bacteria exhibit K_m values of 10-280 nM CH_4 (Knief & Dunfield, 2005), low V_{max} of ~0.1 fmol CH_4 $cell^{-1}$ h^{-1} (Baani & Liesack, 2008) and threshold CH_4 mixing ratios for CH_4 oxidation of ~0.1 ppmv (Bender & Conrad, 1992; Whalen & Reeburgh, 1992; Roslev et al., 1997). The reason for this threshold in CH_4 concentration is still not understood since at this concentration the methanotroph energy yield rate is greater than that estimated for cell maintenance (Kolb et al., 2005). The threshold CH_4 mixing ratios for cell growth, however, have been determined to range from 10 to 100 ppmv for two Methylocytis strains (Knief & Dunfield, 2005). One possible explanation for the apparent CH_4 oxidation threshold observed in some soil studies is that it may reflect a dynamic balance between CH_4 oxidation by methanotrophs and CH_4 production by methanogens as revealed by dual isotope studies (Ambus et al., 2002).

The models used by the Intergovernmental Panel on Climate Change (IPCC AR4) did not account for increases in available SOC due to permafrost thawing or for feedbacks related to permafrost CH_4 emissions (Koven et al., 2011). Models that do take these into account predict greater CH_4 emissions and that the Arctic will become a net source of CO_2 rather than a sink of CO_2 by 2100 (Koven et al., 2011). But even these models may be biased because they have not taken into consideration the results from mineral cryosols sites where atmospheric CH_4 oxidation

has been reported. We, therefore, used a combination of microcosms, stable isotope mass balance, and metagenomic information, to measure the atmospheric CH_4 oxidation rates of a mineral cryosol from the Canadian high Arctic where atmospheric CH_4 uptake has been reported in the field and in the lab (Allan et al., 2014; Stackhouse et al., 2015) and where high-affinity methanotrophic bacteria have been detected (Martineau et al., 2014; Lau et al., 2015). We sought to examine the effects of temperature, water saturation, O_2 potential, light exposure, acetate addition, bicarbonate addition, and depth on the CH_4 oxidation rates and to assess the growth yield of atmospheric CH_4 oxidizers.

Materials and Methods

Field Site

Samples were collected in April 2011 prior to spring thaw from an upland ice-wedge polygon at the McGill Arctic Research Station (MARS) located on Axel Heiberg Island (AHI), Nunavut, Canada (N79°24', W90°45'). Cryosols in this area are classified as acidic (pH 5 – 6.5), static and turbic cryosols and have a sparse coverage of lichen, Salix artica, Polygonum viviparum, and the genera Dryas, Saxifraga, Papaver, and Eriophorum (Stackhouse et al., 2015). The mean annual air temperature (MAAT) is -17.8°C (Pollard, personal communication, 2010). This is one degree warmer than the -18.8°C annual mean air temperature for 2010 of the Eureka weather station approximately one half degree latitude further north (Canadian Climate Normals 1981–2010. Environment Canada. Climate ID: 2401200). During July 2012 air temperatures were observed to reach 15°C and cryosol temperatures ranged from 0°C at the permafrost table to 8°C at the surface. Active layer depth at this location from 2009-2012 has varied between 50-70 cm during maximum active layer development in July. Cryosol SOC was found to vary between 1-6% in the top 10 cm and was <1.5% from 11 cm down to 100 cm depth with a C:N ratio that ranged from 16 to 70 in the top 10 cm and from 15 to 19 from 11 cm to 100 cm (Stackhouse et al., 2015). The $\delta^{13}C$ of the SOC was -26.5±0.5‰ and exhibited no trend with depth (Stackhouse et al., 2015). Undegraded root, stem, and leaf material was observed in the top 10 cm of the cryosol. The 1 m cores were collected into 70% EtOH-sterilized 3" polycarbonate tubes inside of

a SIPRE coring barrel (Jon's Machine Shop, Fairbanks, Alaska), capped, and transported frozen back to Princeton University where they were stored at -20° C until use.

Microcosm preparation

In a 4.5°C cold room a representative frozen core from the polygon interior was partitioned into 10 cm sections using a miter saw sterilized with 70% EtOH. Frozen sections of the core from 0-10 cm (highest SOC content), 30-40 cm (midway point between surface and permafrost), 60-70 (permafrost table), and 70-80 cm (permafrost depth) were chosen for creating microcosms. Core subsections were allowed to thaw on ice for 20 minutes before the outer layer of core sections that had been in contact with the polycarbonate tubing was removed using a sterile knife. Remaining cryosol was placed into Whirl-Pak® bags and placed on ice until thawed. The 10 cm sections were then homogenized by mixing in the Whirl-Pak® bags to avoid subsampling heterogeneous portions of the soil.

The 160 mL serum vials used for the microcosm experiments were pretreated by soaking in 10% HNO_3 overnight, triple-rinsing with distilled H_2O, and then baking at 450°C for 8 hours to remove any organic carbon contamination. To prevent degassing of butyl rubber stoppers into the vials, new stoppers were boiled in 0.1 N NaOH for 1 hour, triple rinsed with distilled H_2O, autoclaved, and then soaked overnight in distilled H_2O following the protocol of Oremland et al. (1987). In a 4.5°C cold room and on ice, 8-10 g of cryosol was placed in the serum vials and capped with stoppers and crimp sealed. Vials were then flushed at 20 PSI for 3 minutes and pressurized to 1.5 atm with a gas mixture containing 400 ppmv CO_2, 1.8 ppmv CH_4, 20% O_2, 80% N_2 (AirGas) for aerobic incubation and with UHP N_2 for anaerobic incubation. Serum vials were covered in aluminum foil to prevent photosynthetic fixation and then incubated in triplicate.

The water content of the mineral cryosol was determined by gravimetric difference after drying the homogenized samples in triplicate at 80°C overnight. Initial water contents of the mineral cryosol were found to be 30.4 ± 2.0% (0-10 cm), 11.0 ± 0.4% (30-40 cm), 8.4 ± 0.6% (60-70 cm), 20.4 ± 0.7% (70-80 cm). Because the highest water holding content (i.e. water saturation) of the cryosol was ~33% H_2O w/w, microcosm experiments were prepared with 33%, 66%, and 100% of water saturation (equating to ~11%, 22%, and 33% H_2O w/w, respectively)

for all depths and incubated in triplicate at 4°C and 10°C in temperature-monitored refrigerators. Experiments that were run with cryosols at below in situ water saturation had cryosol samples dried in a desiccator at 4.5°C without stirring until reaching the desired water content as determined by gravimetric difference. Desiccation required up to 8 days. Although the transition from freezing to 4.5°C during this time may allow for shifts in the microbial community before the experiment began, this was judged to be the least disruptive manner to dry the soils before beginning the microcosm incubations. Cryosols with in situ water content below 66% and 100% saturation level were adjusted to that level using DI H_2O. Treatments were run for 35 (30-40 cm, 70-80 cm), 31 (0-10 cm), 20 (60-70 cm) days.

Anaerobic 70-80 cm cryosol samples were run for 52 days under a headspace of UHP N_2 with the headspace adjusted to either 2.6 ppmv CH_4 or 10 ppmv CH_4 at in situ water saturation (~100%) at both 4°C and 10°C in temperature-monitored refrigerators. Aerobic and anaerobic microcosms were run with vials containing no cryosol additions as controls for outgassing of stoppers, dilution effect due to multiple sampling, and to monitor instrumental drift and potential leakage. The CO_2 and CH_4 concentrations in vials with cryosol were corrected to match the observed change in the controls vials to isolate the microbial signal.

To evaluate the effect of substrate addition and light exposure on CO_2 and CH_4 emissions, three additional sets of microcosm were prepared, using active layer cryosol exposed to light (AL-Light), active layer cryosol in the dark (AL-Dark), and permafrost in the dark (PF). The microcosms contained 5±0.1 g of active layer (AL, 0-10 cm) or permafrost (PF, 70-80 cm) samples. AL-Light and AL-Dark microcosms were incubated under 1.5 atm of ultra-zero grade air (20% O_2, 80% N_2; AirGas, Inc.) containing <10 ppmv CO_2, <50 ppbv CH_4, <30 ppbv CO, and <30 ppbv H_2. After 6 days of incubation, an 8 ppmv CH_4 spike was added to the headspace of the AL-Light and AL-Dark microcosm sets to test for CH_4 oxidation potential. PF microcosms were incubated under 1.5 atm of ultrahigh purity (UHP) N_2 (AirGas Inc.) to test for the methanogenic potential of thawing permafrost. Each microcosm set contained four treatments, without any amendments (in situ), with 2.5 mL of MilliQ water (exceeding the water saturation of the cryosol), 2.5 mL of 1 mM acetate solution (Ac), or 2.5 mL of 1 mM $NaHCO_3$ (Bicarbonate), replicated in duplicate. Preparation and incubation was carried out in a 4.5°C cold room. Vials were flushed again after the addition of amendments and pressurized to 1.5 atm.

Two vials containing no cryosols (blank) were also included as control. All vials were wrapped in aluminum foil and incubated in complete darkness (AL-dark and PF). AL-Light microcosms were incubated under 24 h illumination (Photosynthetic available radiation, PAR = 37 μmol m^{-2} s^{-1}). These microcosms were run for 42 days.

CO_2 and CH_4 Measurements

CO_2 and CH_4 concentrations of the aerobic microcosms were measured by iCO2-CRDS (cavity ring-down spectrometer, Picarro G2101-i CRDS, USA) using a small sample inlet module (SSIM). Measurements were made on injections of 15 mL of gas and headspace was replaced with the original gas mixture to maintain a 1.5 atm pressure inside the vials. Sample injection into the SSIM with the G2101-i coordinator dilutes the sample with 5 mL of ultra-zero grade air (AirGas, Inc.) to bring sample volume up to 20 mL during measurements. Reported concentrations were corrected to account for this dilution. The CH_4 concentrations for anaerobic microcosms were measured by flame ionization (FID) (detection limit ~100 ppbv, FID Peak Performer 1 series, Peak Laboratories, USA) using UHP Argon as a carrier gas, and the CO_2 was measured using a methanizer and FID on the same instrument.

Stable Isotope Experiments

After the initial incubation experiments, those microcosms from 0-10 cm depth exhibiting atmospheric CH_4 oxidation were flushed and pressurized to 1.5 atm with ultra-zero grade air. The vials were then spiked to a concentration of ~10 ppmv with 99% atom labeled $^{13}CH_4$ (^{13}C = $8.8x10^9$ ‰VPDB) and were incubated once more at the original temperatures of 4°C and 10°C. The $\delta^{13}C$-CO_2 and the CO_2 concentrations were measured by CRDS (Picarro G2101-i CRDS, USA) using 20 mL STP of the headspace gas. Isotopic tracer calculations of CH_4 oxidation rates were performed by mass balance, assuming that 1) the $\delta^{13}C$ of CO_2 produced by heterotrophic activity was equal to that of the cryosol SOC $\delta^{13}C$ (-26.5±0.5‰ VPDB) and 2) that all additional ^{13}C-CO_2 was derived from the oxidation of $^{13}CH_4$. The $^{13}C/^{12}C$ ratio of headspace CO_2 was calculated by:

$$\frac{^{13}C}{^{12}C_{CO2}} = \left(\frac{\partial^{13}C_{CO2}}{1000} + 1\right) * \frac{^{13}C}{^{12}C_{VPDB}} \quad (1)$$

where the $^{13}C/^{12}C_{VPDB}$ ratio is 0.0112372. From this the total moles of ^{13}C in the headspace can be calculated by:

$$moles\ ^{13}C_{Total} = \frac{moles\ CO2_{Total} * \frac{^{13}C}{^{12}C_{CO2}}}{\left(1 + \frac{^{13}C}{^{12}C_{CO2}}\right)} \quad (2)$$

The moles of ^{13}C in the headspace derived from oxidation of the SOC are calculated as:

$$moles\ ^{13}C_{From\ soil} = \frac{moles\ CO2_{Total} * \frac{^{13}C}{^{12}C_{Soil}}}{\left(1 + \frac{^{13}C}{^{12}C_{Soil}}\right)} \quad (3)$$

The difference in the total ^{13}C from the ^{13}C expected from SOC degradation is assumed to be the product of CH_4 oxidation to CO_2 by the methanotrophic microbial population since all ^{12}C added to the headspace is assumed to be derived from SOC:

$$moles\ ^{13}C_{Total} - moles\ ^{13}C_{From\ soil} = moles\ ^{13}C_{CH4\ oxidation} \quad (4)$$

This mole abundance was used to determine a rate of CH_4 oxidation independent of the direct measurements of CH_4 consumption in the headspace. CH_4 loss was directly measured by FID using UHP Argon as a carrier gas. CH_4 oxidation rates calculated from the measured headspace CH_4 concentrations were then compared to the rates determined by the shift in $\delta^{13}C$ enrichment of headspace CO_2. The difference between the amount of $^{13}CH_4$ consumed and the amount of $^{13}CO_2$ generated was used to estimate the amount of ^{13}C incorporated into the biomass, assuming that a minor fraction of respired $^{13}CH_4$ was lost to the system as dissolved organic carbon.

Rate Constant Calculations

First order rate constants were calculated for CH_4 oxidation at 4°C and 10°C at 33%, 66%, and 100% water saturation. Constants were determined from the slope of ln [CH_4] versus time

and normalized to cryosol mass, resulting in units of s^{-1} g^{-1}. The slope was calculated from the linear period of active CH_4 oxidation, avoiding any initial lag phase and final threshold level in oxidation. First order reaction rates were also derived by simulation of the results using the Geochemist's Workbench V8.0.12 (Bethke, 2008). Microcosm simulations were carried out for the aerobic 0-10 cm cryosol microcosms under all saturation conditions and for the anaerobic permafrost microcosms. CH_4 consumption was modeled using the following reaction:

$$CH_4 + 2O_2 \rightarrow HCO_3^- + H^+ + H_2O$$

and the following dual-Monod model developed by Jin and Bethke [2003],

$$k = V_{max} [X] F_D F_A F_T \quad (5)$$

where the reaction rate, k is in mol (g of soil)$^{-1}$ s^{-1}, V_{max} is the specific cellular rate for the CH_4 oxidization reaction in mol (mg of biomass)$^{-1}$ s^{-1}, [X] is the methanotroph concentration in mg of biomass (g of soil)$^{-1}$ of the atmospheric CH_4 oxidizers. F_D is the parameter controlling the electron donating reaction rate and was defined by the equation

$$F_D = m_D/(m_D + K_D) \quad (6)$$

where m_D is the concentration of CH_4. Similarly, the electron-accepting reaction rate was controlled by the parameter, F_A, defined by

$$F_A = m_A/(m_A + K_A) \quad (7)$$

where m_A is the concentration of O_2. The terms K_D and K_A represent the half-saturation Michaelis constants, K_m, reported in M units. A V_{max} of 310 nmol g-biomass^{-1} s^{-1} was chosen based on the V_{max} measured by Baani and Liesack (2008) for the high-affinity pMMO of Methylocystis spp. SC2 and assuming a cell dry weight mass of 10^{-13} g cell^{-1} (Phelps et al., 1994). A K_A for O_2 of 0.14 µM was chosen based upon measurements of Type II methanotroph strain OU-4-1 (Joergensen, 1985). A K_D of 0.11 µM was derived from the measurements of Baani and Liesack (2008).

The thermodynamic potential factor, F_T, was used to model the threshold CH_4 concentration where CH_4 oxidation ceased and was defined as

$$F_T = 1 - \exp [-f /(xRT)] \quad (8)$$

where R is the real gas constant 8.314472 J K^{-1} mol^{-1}, T is the temperature in K, x is the average stoichiometric number (Temkin, 1963), or the ratio of the free energy change of the overall reaction to the sum of the free energy changes for each elementary step. For this study we assumed that x was 1 for the reaction stoichiometry as written above. f is the net thermodynamic driving force of the reaction defined by,

$$f = - \Delta G - m \Delta G_p \quad (9)$$

where ΔG is the free energy change of the redox reaction, m is the number of moles of ATP generated per mole of reaction and ΔG_p is the free energy for the phosphorylation reaction ADP + P → ATP (Thauer et al., 1977). For aerobic CH_4 oxidation, ATP is generated by a trans-membrane H^+ gradient created by an electron transport chain. The oxidation of one CH_4 shuttles 9-10 H^+ to the periplasm thereby generating ~3.3 ATP (Bürgmann 2011). The Gibbs free energy for the formation of ATP at 4°C and at a pH of 5 is ~60 kJ (mole of ATP)$^{-1}$ (Larowe and Helgeson, 2007). According to equation 9 this would correspond to a theoretical minimum free energy threshold of ~193 kJ per mole of CH_4 oxidized.

The active biomass concentration was calculated using the following relationship,

$$d[X]/dt = Y\ k - [X]\ D \quad (10)$$

where Y is the yield in mg of biomass mol^{-1} of CH_4 oxidized, which was determined experimentally, k is the reaction rate from equation (5), and D is the death rate in s^{-1}, which in this case was assumed to be zero given the short duration of the experiments.

Simulated CH_4 fugacity was fit to experimental data by utilizing a reaction volume that matched the total CH_4 available in the microcosms, modifying the reaction rate, the initial active biomass, growth yield, ΔG_{ATP} of the reaction, and the thermodynamic potential factor (F_T) of the reaction, while gas concentrations were initialized based on the measured partial pressures. The F_T is threshold free energy below which the reaction ceases (Bethke, 2008). In order to account

for Geochemist's Workbench program not mass balancing the formation of biomass, newly created biomass C was subtracted from the carbon pool at each time step of the model. This resulted in a small decrease of up to 50 ppbv CH_4 from the headspace but did not substantially alter the modeled results. First order reaction constants (k) were calculated from the modeled reaction by dividing the maximum rate of CH_4 oxidation in each microcosm by the dissolved CH_4 concentration at that point and normalized to cryosol mass, resulting in units of s^{-1} g^{-1}. The activation energy for CH_4 oxidation was calculated by multiplying the ideal gas constant (8.314 J K^{-1} mol^{-1}) by the slope of plots of ln(k) against 1000/T(K).

The addition of acetoclastic methanogenesis into the CH_4 oxidation model as an additional source term was tested using the following reaction

$$\text{Acetate} + H_2O \rightarrow CH_4(aq) + HCO_3^- \quad (11)$$

using the parameters of Methanothrix, a K_D of 86 µM (Jetten et al., 1990) and an acetate threshold derived from Westermann et al. (1989).

The CO_2 emission rates were calculated by simply dividing the final CO_2 emitted in moles by the total duration of incubation and the dry weight of the cryosol.

Temperature Response Calculation

The temperature coefficient, Q_{10}, was calculated for the 0-10 cm microcosm incubations by the following formula

$$Q_{10} = \left(\frac{R_2}{R_1}\right)^{\left(\frac{10}{T_2 - T_1}\right)} \quad (52)$$

where R_1 and R_2 stand for the rate of the reaction at the temperatures T_1 and T_2, respectively. Similar to the rate constant calculations, R_1 and R_2 were selected during the period of active oxidation for determining CH_4 oxidation rates.

Cell Count

Cryosol cellular abundances were measured by fluorescent in situ hybridization (FISH). Soil samples were analyzed from frozen cryosol at 5 cm, 35 cm, 65 cm, and ~80 cm with 4 replicates

from each, for a total of 16 samples. For FISH analysis, the following probes were used for eukaryotic cells (EUK516 tagged with Alexa-633 [5′-ACCAGACTTGCCCTCC-3′] targeting eukaryal 18S rRNA genes), archaeal cells (ARC915 tagged with Alexa-555 [5′-GTGCTCCCCCGCCA ATTCCT-3′] targeting archaeal 16S rRNA genes), and bacterial cells (EUB338 tagged with Alexa-594 [5′-GCTGCCTCCCGTAGGAGT- 3′] targeting bacterial 16S rRNA genes). Sample preparation and FISH staining was performed as described (Vishnivetskaya et al., 2014).

Results

CH_4 oxidation

Aerobic incubations - The aerobic CH_4 oxidation rates for the 0-10 cm samples ranged from 16±12 (k=0.003±0.002 g^{-1} d^{-1}) to 260±60 (k=0.036±0.005 g^{-1} d^{-1}) pmol CH_4 gdw^{-1} d^{-1}, with the 10°C and 33% saturation treatment having the highest observed rate of any treatments (ANOVA, p=0.001, Table 2, Fig. 1a). The 10°C and 33% saturation treatment for the 30-40 cm samples also yielded the highest CH_4 oxidation rate for that depth (ANOVA, p=0.005) at 42±3 pmol CH_4 gdw^{-1} d^{-1} (Fig. 1b). The enhancement of the aerobic CH_4 oxidation rate for the 33% saturation treatment was not observed for the 60-70 cm and 70-80 cm samples, nor was it observed for any of the 4°C treatments. Although samples from lower depths exhibited low or no CH_4 oxidation, none of the aerobic incubations produced CH_4 with statistical certainty (Table 2).

The 4°C microcosms showed a consistent delay of ~7 days before CH_4 oxidation began, whereas the 10°C, 33% saturation microcosms exhibited CH_4 oxidation by the third day of incubation and completed CH_4 drawdown within 10 days. CH_4 oxidation ceased at threshold concentrations between 0.1 and 0.5 ppmv CH_4 in the 10°C microcosms and between 0.5 and 1.4 ppmv CH_4 in the 4°C microcosms. The temperature response (Q_{10}) of the 0-10 cm CH_4 oxidation rate was 24.2±12.3 in the 33% saturation samples, 8.3±6.9 in the 66% saturation samples, and 2.4±1.6 in the 100% saturation samples.

For 0-10 cm and 30-40 cm, water saturation and temperature were found to have significant effects on CH_4 oxidation with a significant interaction between the variables such that

the oxidation rate increased with temperature and decreased with water saturation (two-way ANOVA, $p < 0.001$, Table 3). Microcosms from 60-70 cm exhibited significant increases with temperature ($p<0.001$), but did not exhibit any significant effect from water saturation, and no interaction between the two variables was observed (Table 3). Neither temperature nor water saturation level had a significant effect on aerobic CH_4 oxidation in the 70-80 cm samples.

Anaerobic incubations - The anaerobic microcosms of the 70-80 cm cryosols with in situ water saturation levels yielded non-detectable anaerobic CH_4 oxidation (4°C and 10°C with 10 ppmv CH_4; Table 2) to -8.6±1.4 pmol CH_4 gdw^{-1} d^{-1} (4°C and 10°C with 1.8 ppmv CH_4; Table 2). CH_4 production above the concentration of the initial CH_4 spike was not observed in any anaerobic microcosms (Fig. S1g-h). For the 70-80 cm depth, water saturation and temperature were not found to have significant effects on CH_4 oxidation, nor was there a significant interaction between the variables (Table 3).

Light exposure and substrate addition incubations- AL microcosms examining the effects of light and substrate exposure exhibited clear CH_4 consumption. CH_4 oxidation rates were highest in the in situ AL-Light and in situ AL-Dark microcosms (288±123 pmol CH_4 g^{-1} d^{-1} ($k=0.015\pm0.004$ g^{-1} d^{-1}) and 411±70 pmol CH_4 g^{-1} d^{-1} ($k=0.022\pm0.002$ g^{-1} d^{-1}), respectively). Final headspace concentrations of CH_4 ranged from 0.06±0.01 to 3.3±0.3 ppmv. CH_4 oxidation occurred at a higher rate in AL-Dark microcosms for the acetate and bicarbonate treatments ($p=0.02$ and 0.03, respectively) (Fig. 2a). By the end of the experimental run, AL microcosms with amended soils yielded threshold concentrations CH_4 of 1.8-3.2 ppmv , compared to 0.05-0.9 ppmv in AL in situ microcosms. The light versus dark was not quite significant ($p=0.06$) though amendment variables were found to be significant determinants of CH_4 oxidation ($p=0.0004$) and no interactions between the variables were observed ($p=0.4$, Table 3).

Anaerobic PF microcosms containing no CH_4 in the headspace were found to be neither sources nor sinks of CH_4 (Fig. 2a). The methanotrophic rates for the PF microcosms, with or without amendment, were not significantly different (Table 2; Fig. 2), with an average of 3±10 pmol CH_4 g^{-1} d^{-1} averaging across all experimental conditions.

$^{13}CH_4$ oxidation – During the $^{13}CH_4$ incubation experiment, the $^{13}CO_2$ became enriched from -16±6‰ up to 400‰. The directly measured $^{13}CH_4$ oxidation rate of the 0-10 cm sample

was observed to be higher at 10°C than at 4°C (Table 2, p=0.05). No significant differences in the $^{13}CH_4$ oxidation rates were detected between water saturation levels in either the 4°C treatment (p = 0.55) or the 10ºC treatment (p = 0.21). When individual samples were examined, the ratio of expected CH_4 loss from isotopic mass balance of $\delta^{13}C$ of CO_2 to directly observed CH_4 loss was ~0.5 (4°C, slope = 0.46 ± 0.01 R^2 = 0.99; 10°C, slope = 0.56 ± 0.04, R^2 = 0.97) regardless of the total amount of CH_4 being oxidized, indicating that half of oxidized CH_4 remained in the cryosol (Fig. 3a, 3b). Assuming that all of the oxidized CH_4 that did not become CO_2 was incorporated into biomass, this would result in maximal growth yields of 7.4±0.2 g C-biomass mol-CH_4^{-1} at 4°C and 9.0±0.6 g C-biomass mol-CH_4^{-1} at 10°C. The anaerobic $^{13}CH_4$ experiment for the 70-80 cm sample yielded a CH_4 oxidation rate below the detection limit with a shift in the $\delta^{13}C$ of the headspace CO_2 from -17±3‰ to 8±14‰.

CO_2 production

None of the aerobic microcosm experiments exhibited net CO_2 uptake even in the presence of light and all CO_2 emission rates exhibited a two-phase behavior, with a gradual decrease in the emission rates after ~10 days. The CO_2 production rates in the 0-10 cm cryosol samples were the highest among the measured depth profiles (p=0.05) and ranged from 98±17 to 235±150 nmol CO_2 gdw^{-1} d^{-1} with no difference observed between temperature and saturation treatments (p≥0.11) (Table 2, Table 3).

CO_2 production for 66% and 100% water saturation at 60-70 cm and 70-80 cm samples ranged from 34±2 to 44±2 nmol CO_2 gdw^{-1} d^{-1}. The 33% saturation samples at 4ºC and 10ºC for the 30-40 cm, 60-70 cm, and 70-80 cm depths ranged from 13±3 to 37±5 nmol CO_2 gdw^{-1} d^{-1}, though all except for one treatment were below 23 nmol CO_2 gdw^{-1} d^{-1}. These incubations showed no difference as a function of temperature but water saturation level was found to positively correlate with CO_2 emissions (Table 3). An interaction between the variables was found to exist for the 30-40 cm and 60-70 cm microcosms. The temperature response (Q_{10}) of the CO_2 emission rate was 0.9±0.3 for the 33% saturation samples, 2.2±0.8 for the 66% saturation samples, and 3.2±2.0 for the 100% saturation samples.

Anaerobic CO_2 production occurred linearly for the first 35 days at a rate of 36±2 nmol CO_2 gdw^{-1} d^{-1} at 4°C and 47±14 nmol CO_2 gdw^{-1} d^{-1} at 10°C, after which time CO_2 emissions

reduced to near-zero rates until the end of the experiment at 52 days. During the aerobic $^{13}CH_4$ oxidation experiment, the 0-10 cm cryosol CO_2 production rates did not significantly vary by saturation level or by incubation temperature ($p \geq 0.19$, Table 2). The anaerobic $^{13}CH_4$ oxidation experiment yielded CO_2 production rates of 19±5 nmol CO_2 gdw^{-1} d^{-1} at 4ºC and 41±7 nmol CO_2 gdw^{-1} d^{-1} at 10ºC, values in line with the emission rates of aerobic samples below 30 cm but less than those observed in 0-10 cm aerobic samples.

In microcosms examining the effects of light and substrate addition, CO_2 emission rates in PF microcosms oscillated between instantaneous rates of <10 and 70 nmol CO_2 g^{-1} d^{-1}. AL-light microcosms had a higher constant CO_2 emission rate (up to 420±63 nmol CO_2 g^{-1} d^{-1}) than AL-dark microcosms (up to 179±53 nmol CO_2 g^{-1} d^{-1}), with the exception of AL-Light bicarbonate additions (Table 2; Fig. 2b). AL soils produced at least five times more CO_2 than PF soils (Table 2). Exposure to light significantly enhanced CO_2 emissions in the AL microcosms, whereas amendments were not found to have a significant effect on AL or PF microcosms (Table 3).

Microcosm simulations

Data from the $^{13}CH_4$ microcosm experiments in this study indicated a maximum carbon use efficiency of ~50% (8 g-biomass C mol-CH_4^{-1}), which, assuming ~50% C cellular makeup by weight (Bratbak & Dundas, 1984) would result in a growth yield of ~16 grams of biomass per mole of oxidized CH_4. In our modeled CH_4 depletion curves we set the methanotrophic growth yield to 16 grams of biomass per mole of CH_4 oxidized for all conditions.

In fitting the modeled CH_4 oxidation curves to the experimental data the ΔG_p had to be increased from 60 kJ (mole of ATP)$^{-1}$ to 285 to 287 kJ (mole of ATP)$^{-1}$ in order to recreate the threshold CH_4 concentration observed for the 4ºC and 33% water saturation microcosm (Fig. S1; Table S1), otherwise the predicted CH_4 concentrations would decrease to sub-ppt levels. Alternatively models using a balance between methanotrophy and methanogenesis was tried in order to create the observed threshold CH_4 concentrations (Fig. 4). Models incorporating the process of acetoclastic methanogenesis temporarily approximate the threshold value at ~30 days, however this is an inflection point before CH_4 concentration begins to increase again in the

model to over 2 ppmv CH_4, a result not observed in the experimental data (brown curve in Fig. 4). Simple addition of CH_4 into the system at a rate similar to that observed in the anaerobic PF microcosms (equivalent to ~300 pmol CH_4 d^{-1}) was insufficient to reproduce the observed threshold alone and when combined with the ΔG_p of 287 kJ (mole of ATP)$^{-1}$ produced only a marginal increase (orange curve in Fig. 4). Arbitrarily increasing the CH_4 input rates to 100 times the observed value in the anaerobic PF microcosms only created very large initial bursts of CH_4 in the headspace that were not observed in the data and still failed to reproduce the threshold observations (green curve in Fig. 4).

Aerobic CH_4 oxidation rates (Fig. S2a-c) ranged from 0.78 fmol CH_4 (kg-cryosol)$^{-1}$ s^{-1} (4°C 66% saturation) to 9.3 fmol kg-cryosol^{-1} s^{-1} (10°C 33% saturation). Reaction rates at 10°C were 50 to 100% higher than those at 4°C. For the aerobic samples with 2 ppmv CH_4 the calculated activation energies for the microbial CH_4 oxidation rates ranged from 101±57 kJ mol-CH_4^{-1} (pre-exponential factor = $1.7x10^{23}$ nmols of CH_4 g^{-1} d^{-1}) at 33% saturation to 163±159 kJ mol-CH_4^{-1} (pre-exponential factor = $2.6x10^{29}$ nmols of CH_4 g^{-1} d^{-1}) at 100% saturation, with no statistical difference between the treatments. The CH_4 concentrations in the microcosm water in equilibrium with the 2 ppmv CH_4 headspace at 1.5 atmospheres were 7 and 6 nM at 4° and 10°C, respectively. The modeled aerobic CH_4 oxidation rates decreased as the CH_4 concentrations decreased (Fig. S2d-f). As it turns out these rates closely mimic the in situ rates since the original 0-10 cm samples were 100% saturated, the 30-40 cm samples were 33% saturated and the 60-70 and permafrost samples were 66% saturated with water.

Sequence abundance information from metagenomic data gathered from the 5 cm cryosol samples from the same site (Chauhan et al., 2014; Stackhouse et al., 2015) was used to estimate that the total methanotrophic population should account for up to ~1% of the cellular community with a higher proportion of Type II methanotrophs at the surface (~0.8% of total sequences) than in the permafrost (~0.1% of total sequences). Total counts of bacterial, archaeal, and eukaryotic cells determined by FISH averaged $9.8±5.2x10^8$ cells g^{-1}, with bacteria accounting for 82±11% of cell counts and no statistical difference between depths ($p = 0.46$, Fig. S3). Assuming a cell concentration of $9.8x10^8$ cells g^{-1} (Fig. S3) and a 0.8% abundance of Type II methanotrophs, this would result in $7.8x10^6$ Type II methanotrophic-cells g^{-1}. Assuming a cellular mass of $1x10^{-13}$ g cell^{-1} (Phelps et al., 1994) this would equate to ~0.8 mg-biomass kg-cryosol^{-1}. In order to capture

the lag phase of several days in the CH_4 oxidation rate observed in the 4°C treatments, the initial metabolically active biomass had to be set to a lower value of 0.3 ng-biomass kg-cryosol^{-1}. At the end of the simulation the Type II methanotroph biomass was 23 ng-biomass kg-cryosol^{-1}. Assuming $7.8x10^6$ atmospheric CH_4 oxidizing cells g^{-1}, the specific rate of CH_4 oxidation after the lag phase was over ranged from 0.007 fmol CH_4 cell^{-1} day^{-1} (4°C 66% saturation) to 0.08 fmol CH_4 cell^{-1} day^{-1} (10°C 100% saturation) at 2 ppmv CH_4 (Fig. 5, Table 4).

Discussion

The higher CH_4 oxidation rates in the 0-10 cm cryosol samples were likely due to a larger methanotrophic community (1.2% of total sequences) than at depth (<0.5% of total sequences), modulated primarily by increases in Type II methanotrophs (Stackhouse et al., 2015). The lower CH_4 oxidation rates with increasing water saturation for the 10ºC incubations are likely due to limitation of CH_4 and O_2 diffusion through water to the cells (Whalen & Reeburgh, 1996). The lack of a correlation between the CH_4 oxidation rates with increasing water saturation at the 4ºC incubations may reflect the much lower rates of CH_4 oxidation and slightly higher O_2 concentrations due to increased gas solubility, such that O_2 is no longer a limiting factor.

The Q_{10} values for CH_4 oxidation in the 0-10 cm microcosms increased significantly with decreasing water saturation (from 2.4±1.6 to 24.2±12.3), with these high values likely due to the interaction of gas diffusion and temperature rather than simple temperature dependence of CH_4 oxidation alone (Table 3, Davidson & Janssens, 2006). Recent research indicates that the methanotrophic response to warming conditions may be more acute at the lower temperature ranges of polar environments than the temperatures used in our incubation studies (Lupascu et al., 2012; Lau et al., 2015). He et al. (2012) similarly observed increasing CH_4 oxidation rates with increasing temperature in Arctic lake sediments (5-10 µmol CH_4 g^{-1} d^{-1} at 4°C to 35-50 µmol CH_4 g^{-1} d^{-1} at 21°C), as well as a shift in the methanotrophic community towards one with an increased proportion of a Type II methanotroph (genus Methylocystis) in the surface as the temperature increased. He et al. (2012) reported the cooccuring Type I methanotrophs shifted from Methylomonas at 21°C to Methylobacter at 4°C along with the reduction of Methylocystis relative abundance to near zero. Rice paddies also show a strong preference for Type II

methanotrophs closer to the surface, with an increase by a factor of ~2, positively correlating with pore water CH_4 concentrations (Macalady et al., 2002). Knoblauch et al. (2008) found that Siberian polygon (0-5 cm) cryosols with an in situ MAT of -14°C have a CH_4 oxidation rate maximum between 20 and 28°C (~55±20 nmol CH_4 gdw^{-1} h^{-1} compared to ~5±1 nmol CH_4 gdw^{-1} h^{-1} at 0°C). Interestingly, research from the same area in the Lena Delta, Siberia shows that CH_4 oxidation rates exhibit maxima at the surface at high temperature and near the permafrost table at low temperature, indicating that methanotrophic populations had adapted to their long-term in situ temperatures (Liebner & Wagner, 2007). This trend was not observed in the current study.

The 50% CH_4 incorporation value found (Fig. 3) under all temperature and saturation conditions in this study is greater than previously published experiments on methanotrophic isolates reporting growth yields of 8 to 12 grams of biomass per mole of CH_4 oxidized for experiments where the CH_4 concentration ranged from 11,000 to 370,000 ppmv CH_4 and the incubation temperatures ranged from 30°C to 45°C (Vary & Johnson, 1967; Leak & Dalton, 1986a). Our carbon use efficiency, however, is close to the 31 to 43% efficiency reported by Roslev et al. (1997) using $^{14}CH_4$ incubation experiments on atmospheric CH_4 oxidizing soils at a mixing ratios of 5 to 10 ppmv CH_4 and temperatures of 5 and 10°C. It is also comparable to the 31-49% carbon usage efficiency of limiting CH_4 by a Type I methanotrophy in culture (Leak & Dalton, 1986a), and the 45-47% estimated carbon usage efficiency of a methanotroph using nitrate as an N source (Leak & Dalton, 1986b).

Few studies have been conducted testing oxidation rates under atmospheric conditions of 1.8 ppmv CH_4. Experiments at CH_4 concentrations far in excess of those observed in nature may influence observed rates by effectively measuring maximum oxidation rather than in situ oxidation and may be selecting for low-affinity methanotrophs that are not performing the majority of atmospheric CH_4 oxidation in the environment (Dunfield et al., 1999). At atmospheric CH_4 concentrations of 1.8 ppmv and 4° to 10°C, AHI cellular rates (0.007 to 0.08 fmol of CH_4 $cell^{-1}$ day^{-1}) are up to 2-fold higher than those reported for 25°C incubations of Methylocystis, Methylosinus, Methylocaldum, and Methylobacter at 1.8 ppmv CH_4 (Knief & Dunfield, 2005; Baani & Liesack, 2008) (Fig. 2a, Table 5). These isolates had normalized

cellular CH_4 oxidation rates ($cell^{-1}$ day^{-1}) comparable to those of the same cultures grown at CH_4 concentrations up to 1,000 ppmv. Interestingly, the studies with rates comparable to those from this study are both derived from methanotroph batch cultures grown in media continuously shaken by means of a shake plate (Knief & Dunfield, 2005; Baani & Liesack, 2008). A higher oxidation rate for shaken media would be expected since diffusion of CH_4 and O_2 would occur much faster than through static soils (such as the incubation conditions presented here. The cellular CH_4 oxidation rates reported by Liebner and Wagner (2007) for static microcosms using soil subsample (similar to this study) were more than an order of magnitude lower than the results from this study, further highlighting the high affinity of AHI cryosol methanotrophs for CH_4.

The factors determining the threshold concentration for CH_4 oxidation remain unclear. Both the low concentration of H_2 and the lack of increased methanogenesis from acetate amendments argue against substantial hydrogenotrophic or acetoclastic methanogenesis occurring, implying that the steady CH_4 value is not a result of a balance between methanotrophy and methanogenesis. Threshold values were lower at higher temperatures (0.1 to 0.5 ppmv CH_4 at 10°C vs 0.5 to 1.4 ppmv CH_4 at 4°C), and were not clearly correlated with water saturation (Fig. S1). Field observations in Alaska have shown that at lower temperatures (2.5 to 5.5°C) ambient CH_4 concentrations can be maintained at a threshold concentration of 0.1 ppmv (Reeburgh et al., 1997), and that drawdown from up to 50 ppmv CH_4 to near-zero concentrations (T=7°C) can occur on the timescale of tens of hours (Whalen & Reeburgh, 1990). Threshold concentrations closer to those observed in this study were reported by Benstead et al. (1998) (0.5 ppmv CH_4 for Methylobacter and Methylosinus) and Jensen et al. (1998) (0.1 to 0.3 ppmv CH_4), however these microcosms were run with additions of methanol and methanol and formate, respectively. It is possible the methanotrophic strains present at AHI may be facultative methanotrophs capable oxidizing atmospheric CH_4 while using simple carbon compounds other than acetate as cosubstrates. The genome of acidophilic methanotroph Methylocella silvestris (0.53±0.24% sequence abundance at 5 cm) shows it to be capable of using C_1, C_2 (particularly acetate), and C_3 compounds (Chen et al., 2010), whereas the genome of Methylococcus capsulatus (0.10±0.01% sequence abundance at 5 cm) implies some metabolic flexibility and the ability to use simple sugars for metabolic purposes (Ward et al., 2004). The addition of methanol directly to forest soils in situ was found to decrease CH_4 oxidation potential as methanotrophs

using C_1-compounds used that substrate instead (Jensen et al., 1998), a finding that may explain why the acetate addition experiments in this study decreased CH_4 oxidation rates. Regardless, the variable threshold value may be a result of the methanotrophic community adjusting their kinetic properties in response to changing growth conditions and substrate availability (Koch, 1997; Benstead et al., 1998).

Across all saturations, depths, and temperatures, AHI cryosols were able to oxidize CH_4 at atmospheric concentrations, indicating the potential for these cryosols to act as sinks of atmospheric CH_4 with warming. Extrapolating the rates observed here to a surface atmospheric CH_4 uptake yields fluxes ranging from 11.2±6.2 μmol CH_4 m^{-2} d^{-1} (4°C under fully saturated conditions) to 72.6±14.4 μmol CH_4 m^{-2} d^{-1} (10°C under 33% water saturation conditions) (compiled values shown in Table 5). Although these extrapolated fluxes assume that subsurface pore gas contains atmospheric concentrations of CH_4, these values overlap the uptake rates measured in the field with flux chambers (Stackhouse et al. 2015). The CH_4 oxidizing behavior of these cryosols, even under saturated conditions, is in stark contrast to cryosols from other Arctic regions, which are generally reported to be CH_4 sources during full active layer thaw ranging from 40 nmol CH_4 m^{-2} d^{-1} to greater than 25 mmol CH_4 m^{-2} d^{-1} of emissions, across temperatures ranging from 0.5°C to 24°C (Verville et al., 1998; Christensen et al., 2000; Wagner et al., 2005; Mastepanov et al., 2008; Brummell et al., 2012; Lupascu et al., 2012). The 6 orders of magnitude differences could be caused by variations in SOC availability, water saturation, temperature and, also, the balance between methanogenic and methanotrophic activity.

CO_2 production was found to inversely correlate primarily with depth and was highest in the 0-10 cm portion of the core where SOC content and biomass were the highest (Table 2). Although the 66% and 100% saturation treatments were not statistically higher than the 33% treatments, the range and upper bound of CO_2 emissions were larger, indicating that access to carbon substrate may be limited by liquid phase transport in drier soils. Allison and Treseder (2008) observed drying of soils through warming to suppress CO_2 emissions from Alaskan soils and to cause large shifts in the microbial and fungal SOC degrader communities. For the deeper samples the CO_2 production rate appears relatively insensitive to both temperature and water saturation state, perhaps due to the low carbon quality of the ~1% SOC present at these depths (Nadelhoffer et al., 1991; Jagadamma et al., 2014).

The per gram CO_2 production values from these experiments were used to extrapolate a CO_2 flux for these cryosols for the incubation temperatures and saturation conditions on a m^{-2} basis, assuming a soil density of 1.8 g cm^{-3} (Stackhouse et al., 2015) and assuming a deepened active layer depth of 80 cm. The CO_2 production rates measured for the microcosms would correspond to CO_2 emission flux of 52±5 mmol CO_2 m^{-2} d^{-1} under 100 % saturated conditions at 4°C and 41±7 mmol CO_2 m^{-2} d^{-1} at 33% saturation at 10°C (Table 5). Surface fluxes measured at the same locations from which the cryosols samples were collected were 20±5 mmol CO_2 m^{-2} d^{-1} (soil T, 0.7 to 3.6ºC) and 39±26 mmol CO_2 m^{-2} d^{-1} (soil T, 7.9 to 18.4ºC), respectively (Allan et al., 2014). This would be a moderate CO_2 source when compared to summertime active layer fluxes from other sites in the Canadian and Alaskan Arctic, which range from -300 to 500 mmol CO_2 m^{-2} d^{-1} (Verville et al., 1998; Williams et al., 2000; Worthy & Levin, 2000; Brummell et al., 2012; Stackhouse et al., 2015).

Critical questions remain, however, as to the long-term duration of these responses to temperature and saturation. Future studies examining the microbial response and geochemical evolution of long-term changes in mineral cryosol permafrost systems will provide essential information for modeling the Arctic carbon cycle through the rest of the century.

Conclusion

The atmospheric CH_4 oxidation rates were measured in microcosms incubated at 4°C and 10°C along a 1 m depth profile and over a range of water saturation conditions for mineral cryosols containing Type I and Type II methanotrophs from Axel Heiberg Island (AHI), Nunavut, Canada. Our research indicates that for cryosols derived from Axel Heiberg Island the following parameters impact CH_4 uptake and CO_2 emission rates:

1. Increasing water saturation, while limiting CH_4 oxidation in cryosols, does not eliminate it or result in net CH_4 emissions. Increasing water saturation was not found to have a significant effect on CO_2 emissions from cryosols.

2. CH_4 oxidation was increased by roughly a factor of 2 for samples from the active layer (0-70 cm) by a shift in temperature from 4°C to 10°C. A similar trend held true for CO_2 emissions only for the top 10 cm, where SOC content was the highest.
3. CH_4 oxidation from Axel Heiberg cryosols is able to occur at a higher cellular rate than many other Arctic sites when accounting for temperature and CH_4 concentration of incubation, indicating that methanotrophs at this site have a high affinity for CH_4. Biomass incorporation of oxidized CH_4 was shown at 10 ppmv CH_4, suggesting that AHI methanotrophs may be able to grow on CH_4 at this concentration.

The cryosols exhibited net consumption of 1.8 ppmv CH_4 under all conditions, including during anaerobic incubations. Methane oxidation rates increased with temperature and decreased with increasing water saturation at 10ºC and depth, exhibiting the highest rates at 10°C and 33% saturation at 5 cm depth (260±60 pmol CH_4 gdw^{-1} d^{-1}). The CH_4 oxidation rates for the 4ºC incubations, however, did not vary significantly with water saturation. Extrapolation of the CH_4 oxidation rates to the field yields net CH_4 uptake rates ranging from 11 to 73 µmol CH_4 m^{-2} d^{-1}, which are comparable to field measurements. Stable isotope mass balance indicates ~50% of the oxidized CH_4 is incorporated into the methanotrophic biomass at a CH_4 concentration of only 10 ppmv, regardless of temperature or saturation. Future atmospheric CH_4 uptake rates at AHI with increasing temperatures will be determined by the interplay of increasing CH_4 oxidation rates versus water saturation and the depth to the water table during summer thaw. CO_2 production was found to inversely correlate primarily with depth and was highest in the 0-10 cm portion of the core where SOC content and biomass were the highest. Thawing of high SOC permafrost cryosols can lead to rapid changes in the microbial community and metabolic pathways (Mackelprang et al., 2011) and in the degradation of SOC (Coolen et al., 2011), affecting the substrates available for metabolism. Although the availability of soil C and N stores has been shown to enhance CH_4 production in high SOC Alaskan soils (Waldrop et al., 2010) the direct addition of acetate had no effect on either net CH_4 oxidation or production in this study (Fig. 2, Table 3).

Acknowledgements

This research was funded by U. S. Department of Energy Office of Science, Office of Biological and Environmental Research, Genomic Science Program (No. DE-SC0004902) to T.C.O. and logistical support was provided by the Canadian Polar Continental Shelf Program to L. Whyte of McGill University. Field assistance during sample collection was provided by G. Lamarche-Gagnon, R. Wilhelm, and N. Mykytczuk of McGill University.

References

Adachi K, Ohtsuka T, Nakatsubo T, Koizumi H (2006) The methane flux along topographical gradients on a glacier foreland in the High Arctic, Ny-Ålesund, Svalbard. Polar Biosci **20**, 131–139.

Allan J, Ronholm J, Mykytczuk NS, Greer CW, Onstott TC, Whyte LG (2014) Methanogen community composition and rates of methane consumption in Canadian High Arctic permafrost soils. Environmental Microbiology Reports.

Allison SD, Treseder KK (2008) Warming and drying suppress microbial activity and carbon cycling in boreal forest soils. Global Change Biology **14**, 2898–2909.

Allison SD, Wallenstein MD, Bradford MA (2010) Soil-carbon response to warming dependent on microbial physiology. Nature Geoscience **3**, 336–340.

Ambus P, Andersen BL, Kemner M, Sørensen B, Wille J (2002) Natural carbon isotopes used to study methane consumption and production in soil. Isotopes in environmental and health studies **38**, 149–157.

Baani M, Liesack W (2008) Two isozymes of particulate methane monooxygenase with different methane oxidation kinetics are found in Methylocystis sp. strain SC2. Proceedings of the National Academy of Sciences **105**, 10203–8.

Bäckstrand K, Crill PM, Jackowicz-Korczyñski M, Mastepanov M, Christensen TR, Bastviken D (2010) Annual carbon gas budget for a subarctic peatland, Northern Sweden. Biogeosciences **7**, 95–108.

Bárcena TG, Finster KW, Yde JC (2011) Spatial Patterns of Soil Development, Methane Oxidation, and Methanotrophic Diversity along a Receding Glacier Forefield, Southeast Greenland. Arctic, Antarctic, and Alpine Research **43**, 178–188.

639 Bender M, Conrad R (1992) Kinetics of CH 4 oxidation in oxic soils exposed to ambient air or
640 high CH 4 mixing ratios. FEMS Microbiology Letters **101**, 261–269.

641 Benstead J, King GM, Williams HG (1998) Methanol promotes atmospheric methane oxidation
642 by mathanotrophic cultures and soils **64**, 1091–1098.

643 Bethke CM (2008) Geochemical and Biogeochemical Reaction Modeling, 2nd editio. University
644 of Illinois, Urbana, Illinois.

645 Bratbak G, Dundas I (1984) Bacterial dry matter content and biomass estimations. Applied and
646 environmental microbiology **48**, 755–757.

647 Brummell ME, Farrell RE, Hardy SP, Siciliano SD (2014) Greenhouse gas production and
648 consumption in High Arctic deserts. Soil Biology and Biochemistry **68**, 158–165.

649 Brummell ME, Farrell RE, Siciliano SD (2012) Greenhouse gas soil production and surface
650 fluxes at a high arctic polar oasis. Soil Biology and Biochemistry **52**, 1–12.

651 Chauhan A, Layton AC, Vishnivetskaya TA, Williams D, Pfiffner SM, Rekepalli B (2014)
652 Metagenomes from Thawing Low-Soil-Organic-Carbon Mineral Cryosols and Permafrost of the
653 Canadian High Arctic. Genome Announcements **2**, 1–2.

654 Chen Y, Crombie A, Rahman MT, Dedysh SN, Liesack W, Stott MB, Alam M, Theisen AR,
655 Murrell JC, Dunfield PF (2010) Complete genome sequence of the aerobic facultative
656 methanotroph Methylocella silvestris BL2. Journal of bacteriology **192**, 3840–1.

657 Christensen T, Friborg T, Sommerkorn M, Kaplan J, Illeris L, Soegaard H, Nordstroem C,
658 Jonasson S (2000) Trace gas exchange in a high Arctic valley: 1. Variations in CO2 and CH4
659 Flux between tundra vegetation types. Global Biogeochemical Cycles **14**, 701–713.

660 Christensen T, Jonasson S, Callaghan T, Havstrom M (1995) Spatial variation in high-latitude
661 methane flux along a transect across Siberian and European tundra environments. Journal of
662 Geophysical Research **100**, 21035–21045.

663 Coolen MJL, Giessen J van de, Zhu EY, Wuchter C (2011) Bioavailability of soil organic matter
664 and microbial community dynamics upon permafrost thaw. Environmental microbiology **13**,
665 2299–314.

Davidson E, Janssens I (2006) Temperature sensitivity of soil carbon decomposition and feedbacks to climate change. Nature **440**, 165–73.

Degelmann DM, Borken W, Drake HL, Kolb S (2010) Different atmospheric methane-oxidizing communities in European beech and Norway spruce soils. Applied and environmental microbiology **76**, 3228–35.

Dlugokencky EJ, Lang PM, Crotwell AM, Masarie KA, Crotwell M. (2014) Atmospheric Methane Dry Air Mole Fractions from the NOAA ESRL Carbon Cycle Cooperative Global Air Sampling Network, 1983-2013 2014–06–24.

Dunfield P, Liesack W, Henckel T, Knowles R, Conrad R (1999) High-affinity methane oxidation by a soil enrichment culture containing a type II methanotroph. Applied and environmental microbiology **65**, 1009–1014.

Emmerton CA, Louis VL St., Lehnherr I, Humphreys ER, Rydz E, Kosolofski HR (2014) The net exchange of methane with high Arctic landscapes during the summer growing season. Biogeosciences Discussions **11**, 1673–1706.

Girguis P, Orphan V, Hallam S, DeLong E (2003) Growth and methane oxidation rates of anaerobic methanotrophic archaea in a continuous-flow bioreactor. Applied and environmental microbiology **69**, 5472–5482.

Graef C, Hestnes AG, Svenning MM, Frenzel P (2011) The active methanotrophic community in a wetland from the High Arctic. Environmental microbiology reports **3**, 466–72.

Graham DE, Wallenstein MD, Vishnivetskaya T a, Waldrop MP, Phelps TJ, Pfiffner SM, Onstott TC, Whyte LG, Rivkina EM, Gilichinsky DA, Elias DA, Mackelprang R, VerBerkmoes NC, Hettich RL, Wagner D, Wullschleger SD, Jansson JK (2012) Microbes in thawing permafrost: the unknown variable in the climate change equation. The ISME journal **6**, 709–12.

Grosse G, Harden J, Turetsky M, McGuire AD, Camill P, Tarnocai C, Frolking S, Schuur E a G, Jorgenson T, Marchenko S, Romanovsky V, Wickland KP, French N, Waldrop M, Bourgeau-Chavez L, Striegl RG (2011) Vulnerability of high-latitude soil organic carbon in North America to disturbance. Journal of Geophysical Research: Biogeosciences **116**, 1–23.

Hayes DJ, Kicklighter DW, McGuire AD, Chen M, Zhuang Q, Yuan F, Melillo JM,

694 Wullschleger SD (2014) The impacts of recent permafrost thaw on land–atmosphere greenhouse
695 gas exchange. Environmental Research Letters **9**, 045005.

696 He R, Wooller MJ, Pohlman JW, Quensen J, Tiedje JM, Leigh MB (2012) Shifts in identity and
697 activity of methanotrophs in arctic lake sediments in response to temperature changes. Applied
698 and environmental microbiology **78**, 4715–23.

699 Hill GB, Henry GHR (2011) Responses of High Arctic wet sedge tundra to climate warming
700 since 1980. Global Change Biology **17**, 276–287.

701 Hugelius G, Strauss J, Zubrzycki S, Harden JW, Schuur EAG, Ping CL, Schirrmeister L, Grosse
702 G, Michaelson GJ, Koven CD, O'Donnell JA, Elberling B, Mishra U, Camill P, Yu Z, Palmtag J,
703 Kuhry P (2014) Improved estimates show large circumpolar stocks of permafrost carbon while
704 quantifying substantial uncertainty ranges and identifying remaining data gaps. Biogeosciences
705 Discussions **11**, 4771–4822.

706 Jagadamma S, Mayes M a., Steinweg JM, Schaeffer SM (2014) Substrate quality alters the
707 microbial mineralization of added substrate and soil organic carbon. Biogeosciences **11**, 4665–
708 4678.

709 Jensen S, Priemé A, Bakken L (1998) Methanol improves methane uptake in starved
710 methanotrophic microorganisms. Applied and Environmental Microbiology **64**, 1143–1146.

711 Jetten MSM, Stams AJM, Zehnder AJB (1990) Acetate threshold values and acetate activating
712 enzymes in methanogenic bacteria. FEMS Microbiology Letters **73**, 339–344.

713 Jin Q, Bethke CM (2003) A new rate law describing microbial respiration. Applied and
714 Environmental Microbiology **69**, 2340–2348.

715 Joergensen L (1985) The methane mono-oxygenase reaction system studied in vivo by
716 membrane-inlet mass spectrometry. The Biochemical Journal **225**, 441–8.

717 Jorgenson MT, Shur YL, Pullman ER (2006) Abrupt increase in permafrost degradation in
718 Arctic Alaska. Geophysical Research Letters **33**, L02503.

719 Knief C, Dunfield PF (2005) Response and adaptation of different methanotrophic bacteria to
720 low methane mixing ratios. Environmental microbiology **7**, 1307–17.

Knoblauch C, Zimmermann U, Blumenberg M, Michaelis W, Pfeiffer E (2008) Methane turnover and temperature response of methane-oxidizing bacteria in permafrost-affected soils of northeast Siberia. Soil Biology and Biochemistry **40**, 3004–3013.

Koch A (1997) Microbial physiology and ecology of slow growth. Microbiology and molecular biology reviews **61**, 305–318.

Kolb S (2009) The quest for atmospheric methane oxidizers in forest soils. Environmental microbiology reports **1**, 336–46.

Kolb S, Knief C, Dunfield PF, Conrad R (2005) Abundance and activity of uncultured methanotrophic bacteria involved in the consumption of atmospheric methane in two forest soils. Environmental Microbiology **7**, 1150–1161.

Koven CD, Ringeval B, Friedlingstein P, Ciais P, Cadule P, Khvorostyanov D, Krinner G, Tarnocai C (2011) Permafrost carbon-climate feedbacks accelerate global warming. Proceedings of the National Academy of Sciences of the United States of America **108**, 14769–74.

Lau MCY, Stackhouse BT, Layton AC, Chauhan A, Vishnivetskaya TA, Chourey K, Ronholm J, Mykytczuk NCS, Bennett PC, Lamarche-Gagnon G, Burton N, Pollard WH, Omelon CR, Medvigy DM, Hettich RL, Pfiffner SM, Whyte LG, Onstott TC (2015) An active atmospheric methane sink in high Arctic mineral cryosols. The ISME Journal.

Lawrence DM, Slater AG, Romanovsky VE, Nicolsky DJ (2008) Sensitivity of a model projection of near-surface permafrost degradation to soil column depth and representation of soil organic matter. Journal of Geophysical Research **113**, F02011.

Leak D, Dalton H (1986a) Growth yields of methanotrophs 1. Applied microbiology and biotechnology **23**, 470–476.

Leak D, Dalton H (1986b) Growth yields of methanotrophs 2: A theoretical analysis. Applied microbiology and biotechnology **23**, 477–481.

Liebner S, Wagner D (2007) Abundance, distribution and potential activity of methane oxidizing bacteria in permafrost soils from the Lena Delta, Siberia. Environmental microbiology **9**, 107–17.

Liebner S, Zeyer J, Wagner D, Schubert C, Pfeiffer E-M, Knoblauch C (2011) Methane

oxidation associated with submerged brown mosses reduces methane emissions from Siberian polygonal tundra. Journal of Ecology **99**, 914–922.

Lupascu M, Wadham J, Hornibrook E, Pancost R (2012) Temperature Sensitivity of Methane Production in the Permafrost Active Layer at Stordalen, Sweden: A Comparison with Non-permafrost Northern Wetlands. Arctic, Antarctic, and Alpine Research **44**, 469–482.

Macalady JL, McMillan AMS, Dickens AF, Tyler SC, Scow KM (2002) Population dynamics of type I and II methanotrophic bacteria in rice soils. Environmental Microbiology **4**, 148–157.

Mackelprang R, Waldrop MP, DeAngelis KM, David MM, Chavarria KL, Blazewicz SJ, Rubin EM, Jansson JK (2011) Metagenomic analysis of a permafrost microbial community reveals a rapid response to thaw. Nature **480**, 368–71.

Martineau C, Pan Y, Bodrossy L, Yergeau E, Whyte LG, Greer CW (2014) Atmospheric methane oxidizers are present and active in Canadian high Arctic soils. FEMS microbiology ecology 1–13.

Mastepanov M, Sigsgaard C, Dlugokencky EJ, Houweling S, Ström L, Tamstorf MP, Christensen TR (2008) Large tundra methane burst during onset of freezing. Nature **456**, 628–30.

Montzka S, Dlugokencky E, Butler J (2011) Non-CO2 greenhouse gases and climate change. Nature **476**, 43–50.

Nadelhoffer K, Giblin A, Shaver G, Laundre J (1991) Effects of temperature and substrate quality on element mineralization in six arctic soils. Ecology **72**, 242–253.

Ohtsuka T, Adachi M, Uchida M, Nakatsubo T (2006) Relationships between vegetation types and soil properties along a topographical gradient on the northern coast of the Brøgger Peninsula, Svalbard. Polar Bioscience **19**, 63–72.

Oremland R, Miller L, Whiticar M (1987) Sources and flux of natural gases from Mono Lake, California. Geochimica et Cosmochimica Acta **51**, 2915–2929.

Osterkamp TE (2007) Characteristics of the recent warming of permafrost in Alaska. Journal of Geophysical Research **112**, F02S02.

Phelps TJ, Murphy EM, Pfiffner SM, White DC (1994) Comparison between geochemical and biological estimates of subsurface microbial activities. Microbial ecology **28**, 335–49.

Reeburgh WS, Hirsch a I, Sansone FJ, Popp BN, Rust TM (1997) Carbon kinetic isotope effect accompanying microbial oxidation of methane in boreal forest soils. Geochimica et Cosmochimica Acta **61**, 4761–4767.

Roslev P, Iversen N, Henriksen K (1997) Oxidation and assimilation of atmospheric methane by soil methane oxidizers. Applied and environmental microbiology **63**, 874–80.

Rowlands DJ, Frame DJ, Ackerley D, Aina T, Booth BBB, Christensen C, Collins M, Faull N, Forest CE, Grandey BS, Gryspeerdt E, Highwood EJ, Ingram WJ, Knight S, Lopez A, Massey N, McNamara F, Meinshausen N, Piani C, Rosier SM, Sanderson BM, Smith LA, Stone DA, Thurston M, Yamazaki K, Hiro Yamazaki Y, Allen MR (2012) Broad range of 2050 warming from an observationally constrained large climate model ensemble. Nature Geoscience **5**, 256–260.

Sachs T, Wille C, Boike J, Kutzbach L (2008) Environmental controls on ecosystem-scale CH 4 emission from polygonal tundra in the Lena River Delta, Siberia. Journal of Geophysical Research **113**, G00A03.

Schuur EAG, Bockheim J, Canadell JG, Euskirchen E, Field CB, Goryachkin S V., Hagemann S, Kuhry P, Lafleur PM, Lee H, Mazhitova G, Nelson FE, Rinke A, Romanovsky VE, Shiklomanov N, Tarnocai C, Venevsky S, Vogel JG, Zimov SA (2008) Vulnerability of Permafrost Carbon to Climate Change: Implications for the Global Carbon Cycle. BioScience **58**, 701.

Shindell DT, Faluvegi G, Koch DM, Schmidt GA, Unger N, Bauer SE (2009) Improved attribution of climate forcing to emissions. Science (New York, N.Y.) **326**, 716–718.

Stackhouse BT, Vishnivetskaya TA, Layton A, Chauhan A, Pfiffner S, Mykytczuk NC, Sanders R, Whyte LG, Hedin L, Saad N, Myneni S, Onstott TC (2015) Simulated spring thaw of permafrost from mineral cryosol reveals increase in CO2 emissions and an atmospheric CH4 sink. Journal of Geophysical Research: Biogeosciences **In press**, n/a–n/a.

Temkin MI (1963) Kinetics of stationary reactions. Proceedings of the USSR Academy of

Sciences **152**, 156–159.

Thauer RK, Jungermann K, Decker K (1977) Energy conservation in chemotrophic anaerobic bacteria. Bacteriological reviews **41**, 100–180.

Vary P, Johnson M (1967) Cell yields of bacteria grown on methane. Applied microbiology **15**, 1473–1478.

Verville J, Hobbie S, Chapin III F, Hooper D (1998) Response of tundra CH4 and CO2 flux tomanipulation of temperature and vegetation. Biogeochemistry **4**, 215–235.

Vishnivetskaya T a, Layton AC, Lau MCY, Chauhan A, Cheng KR, Meyers AJ, Murphy JR, Rogers AW, Saarunya GS, Williams DE, Pfiffner SM, Biggerstaff JP, Stackhouse BT, Phelps TJ, Whyte L, Sayler GS, Onstott TC (2014) Commercial DNA extraction kits impact observed microbial community composition in permafrost samples. FEMS microbiology ecology **87**, 217–30.

Wagner D, Kobabe S, Pfeiffer E-M, Hubberten H-W (2003) Microbial controls on methane fluxes from a polygonal tundra of the Lena Delta, Siberia. Permafrost and Periglacial Processes **14**, 173–185.

Wagner D, Lipski A, Embacher A, Gattinger A (2005) Methane fluxes in permafrost habitats of the Lena Delta: effects of microbial community structure and organic matter quality. Environmental microbiology **7**, 1582–92.

Waldrop MP, Wickland KP, White R, Berhe a. a., Harden JW, Romanovsky VE (2010) Molecular investigations into a globally important carbon pool: Permafrost-protected carbon in Alaskan soils. Global Change Biology **16**, 2543–2554.

Walter KM, Zimov S, Chanton JP, Verbyla D, Chapin FS (2006) Methane bubbling from Siberian thaw lakes as a positive feedback to climate warming. Nature **443**, 71–5.

Ward N, Larsen Ø, Sakwa J, Bruseth L, Khouri H, Durkin a S, Dimitrov G, Jiang L, Scanlan D, Kang KH, Lewis M, Nelson KE, Methé B, Wu M, Heidelberg JF, Paulsen IT, Fouts D, Ravel J, Tettelin H, Ren Q, Read T, DeBoy RT, Seshadri R, Salzberg SL, Jensen HB, Birkeland NK, Nelson WC, Dodson RJ, Grindhaug SH, Holt I, Eidhammer I, Jonasen I, Vanaken S, Utterback T, Feldblyum T V, Fraser CM, Lillehaug JR, Eisen J a (2004) Genomic insights into

methanotrophy: the complete genome sequence of Methylococcus capsulatus (Bath). PLoS biology **2**, e303.

Westermann P, Ahring BK, Mah R a (1989) Threshold acetate concentrations for acetate catabolism by aceticlastic methanogenic bacteria. Applied and environmental microbiology **55**, 514–515.

Whalen S, Reeburgh W (1992) Interannual variations in tundra methane emission: A 4-year time series at fixed sites. Global Biogeochemical Cycles **6**, 139–159.

Whalen S, Reeburgh W (1996) Moisture and temperature sensitivity of CH4 oxidation in Boreal soils. Soil Biology and Biochemistry **28**, 1271–1281.

Whalen SC, Reeburgh WS (1990) Consumption of atmospheric methane by tundra soils. Nature **346**, 160–162.

Williams M, Eugster W, Rastetter E, McFadden J, III FC (2000) The controls on net ecosystem productivity along an Arctic transect: a model comparison with flux measurements. Global Change Biology **6**, 116–126.

Worthy D, Levin I (2000) Evidence for a link between climate and northern wetland methane emissions. Journal of Geophysical Research **105**, 4031–4038.

Fig. legends

Fig. 1.

Fig. 1. The average of triplicate CH_4 oxidation rates at 4°C and 10°C as a function of water saturation for (a) 0-10 cm, (b) 30-40 cm, (c) 60-70 cm, (d) 70-80 cm. Error bars represent ± 1 S.D.

Fig. 2

Fig. 2. CH_4 oxidation rates and CO_2 emission rates for microcosms incubated at 4.5ºC and examining light versus dark response and response to acetate, bicarbonate and water amendments. Negative values indicate uptake CH_4 into the soil. Error bars represent ± 1 S.D.

Fig. 3

Fig. 3 Caption: (a) 4°C and (b) 10°C comparison between observed and expected CH_4 loss based on direct measurements and isotopic tracer methods. 4°C (m = 0.47±0.01, R^2 = 0.99); 10°C (m = 0.56±0.04, R^2 = 0.97). Error bars represent ± 1 S.D.

Fig. 4

Fig. 4. The results of different modeling components overlain on the experimental results from the 4°C 33% saturation microcosm. MT stands for the methanotrophy only model. MT + AcMG stands for the methanotrophy model with acetoclastic methanogenesis added. MT + 300 pmol CH_4 d^{-1} is the methanotrophy model with 300 pmol CH_4 added into the system daily. MMT + 30 nmol CH_4 d^{-1} represents a methanotrophy model with a lowered CH_4 oxidation activation energy and 30 nmol CH_4 added into the system daily. Error bars represent ± 1 S.D.

Fig. 5

Fig. 5. Cellular oxidation rates normalized to concentration of CH_4 as a function of (a) CH_4 concentration and (b) temperature compared to values calculated from the literature.

Methanotrophs being compared are Methylocystis sp. Strain SC2 (Type II) (Baani & Liesack, 2008), Methylocystis and Methylosinus (Type II) and Methylocaldum and Methlyobacter (Type II) (Knief & Dunfield, 2005), Anaerobic CH_4 oxidation by marine sediments from CH_4 seep (ANME-2c) (Girguis et al., 2003), and an environmental mix of Type I and II from 30 cm depth polygon soil from Lena Delta, Russia (Liebner & Wagner, 2007).

Fig. S1

Fig. S1. Measured (diamonds) and modeled (line) CH_4 headspace depletion during the course of soil incubations. Error bars represent ± 1 S.D. Where no error bars are visible the symbol is larger than the error.

Fig. S2

Fig. S2. Reaction rates and thermodynamic potential factor (F_T, eq. 8) of surface soil (0-10 cm) microcosm conditions and permafrost soil (70-80 cm) microcosm conditions.

Fig. S3

Fig. S3. Estimation of cellular abundances of a depth profile by the FISH.

Tables

Table 1. Soil organic carbon content and in situ CH_4 fluxes from cryosol soil surfaces from sites across the Arctic.

Location	SOC (%)	CH_4 Oxidation Rate	Reference
Lena Delta, Siberia	2-18	2.2 - 7.5 mmol CH_4 m^{-2} d^{-1}	(Wagner et al., 2003, 2005; Sachs et al., 2008)
Samoylov, Siberia	20-39	-835 nmol CH_4 m^{-2} d^{-1} *	(Knoblauch et al., 2008)
Stordalen, Sweden	24-59	0.04 - 9.9 mmol CH_4 m^{-2} d^{-1}	(Bäckstrand et al., 2010; Lupascu et al., 2012)
Zackenberg Valley, Greenland	NR	1.4 - 25.5 mmol CH_4 m^{-2} d^{-1}	(Mastepanov et al., 2008)
Ellesmere Island, Nunavut	15-22	-1.5 - 3.1 µmol CH_4 m^{-2} d^{-1}	(Hill & Henry, 2011; Brummell et al., 2012)
Unalaska Island, Alaska	16-36	-0.17 mmol CH_4 m^{-2} d^{-1}	(Whalen & Reeburgh, 1990)
Siberian polygons and bogs	6-95	0.14 - 2.9 mmol CH_4 m^{-2} d^{-1}	(Christensen et al., 1995)
Spitsbergen, Svalbard	3-26	-0.5 - -0.29 nmol CH_4 g^{-1} d^{-1}	(Ohtsuka et al., 2006; Graef et al., 2011)
Ammassalik Island, Greenland	<1	-2.1 nmol CH_4 g^{-1} d^{-1}	(Bárcena et al., 2011)
Samoylov Island, Siberia	NR	-0.1 - 1.4 mmol CH_4 m^{-2} d^{-1}	(Liebner et al., 2011)
Axel Heiberg Island, Nunavut	1-5	-9.4 µmol CH_4 m^{-2} d^{-1}	(Allan et al., 2014)

* indicates that CH_4 fluxes were determined from experiments using higher than atmospheric CH_4 concentrations. Negative values indicate CH_4 uptake by the soils.

906 Table 2. CO_2 emission and CH_4 oxidation rates from aerobic and anaerobic microcosms.

Aerobic 1.8 ppm CH_4	**0-10 cm**		**30-40 cm**		**60-70 cm**		**70-80 cm**	
	CO_2 (nmol gdw^{-1} d^{-1})		CO_2 (nmol gdw^{-1} d^{-1})		CO_2 (nmol gdw^{-1} d^{-1})		CO_2 (nmol gdw^{-1} d^{-1})	
% Saturation	4° C	10° C	4° C	10° C	4° C	10° C	4° C	10° C
33	106 ± 26	98 ± 17	22*	13 ± 3	20 ± 1	37 ± 5	19 ± 7	21 ± 5
66	142 ± 16	222 ± 77	19 ± 1	22 ± 6	42 ± 5	37 ± 2	37 ± 2	38 ± 8
100	125 ± 14	235 ± 150	16 ± 2	21 ± 2	44 ± 2	40 ± 5	34 ± 2	36 ± 18

	0-10 cm		**70-80 cm**
	CO_2 (nmol g^{-1} d^{-1})		
Treatment	AL Light	AL Dark	PF Dark (anaerobic)
in situ*	252 ± 110	105 ± 23	29 ± 6
Water*	420 ± 63	179 ± 53	34 ± 28
Acetate*	413 ± 84	111 ± 9	3 ± 2
Bicarbonate*	105 ± 15	156 ± 44	7 ± 1

$^{13}CH_4$ microcosms	**0-10 cm**	
	CO_2 (nmol g^{-1} d^{-1})	
% Saturation	4° C	10° C
33	63 ± 26	55 ± 3
66	75 ± 14	95 ± 15
100	71 ± 10	151 ± 96

Aerobic 1.8 ppm CH_4	**0-10 cm**		**30-40 cm**		**60-70 cm**		**70-80 cm**	
	CH_4 (pmol gdw^{-1} d^{-1}) (k (g^{-1} d^{-1}))		CH_4 (pmol gdw^{-1} d^{-1}) (k (g^{-1} d^{-1}))		CH_4 (pmol gdw^{-1} d^{-1}) (k (g^{-1} d^{-1}))		CH_4 (pmol gdw^{-1} d^{-1}) (k (g^{-1} d^{-1}))	
% Saturation	4° C	10° C	4° C	10° C	4° C	10° C	4° C	10° C
33	-44 ± 20 (-0.011±0.006)	-260 ± 60 (-0.036±0.005)	-2.9* (-0.0002)	-42.4 ± 2.7 (-0.0013±0.0004)	0.3 ± 1.9 (-0.0001±0.0001)	-7.3 ± 1.8 (0.0001±0.0001)	-7.2 ± 2.7 (-0.0002±0.0001)	-1.6 ± 9.0 (-0.0005±0.0003)
66	-16 ± 12 (-0.003±0.002)	-53 ± 18 (-0.004±0.002)	-3.2 ± 1.7 (-0.001±0.0007)	-15.7 ± 2.6 (-0.0012±0.0003)	-1.2 ± 1.9 (-0.00001±0.0001)	-8.0 ± 0.4 (0.0004±0.0001)	-10.0 ± 3.4 (-0.0003±0.0003)	0.1 ± 2.2 (-0.0001±0.0001)
100	-34 ± 19 (-0.002±0.001)	-54 ± 18 (-0.005±0.004)	-7.5 ± 4.5 (-0.0015±0.0009)	-18.7 ± 11.3 (-0.0017±0.0001)	-0.7 ± 1.0 (0.0001±0.0001)	-6.0 ± 2.0 (0.0002±0.0001)	-6.0 ± 0.4 (-0.0001±0.0002)	-6.6 ± 10.8 (-0.001±0.0004)

	0-10 cm		**70-80 cm**
	CH_4 (pmol g^{-1} d^{-1})**		
Treatment	AL Light	AL Dark	PF Dark (anaerobic)
in situ*	-288 ± 123 (-0.015±0.004)	-411 ± 70 (-0.022±0.002)	-6 ± 1 NA
Water*	-105 ± 11 (-0.0055±0.0003)	-119 ± 2 (-0.0062±0.0001)	-4 ± 2 NA
Acetate*	-86 ± 2 (-0.0045±0.0001)	-157 ± 16 (-0.0082±0.0005)	-2 ± 3 NA
Bicarbonate*	-112 ± 1 (-0.0058±0.0001)	-129 ± 4 (-0.0067±0.0001)	0 ± 1 NA

		0-10 cm***	
		CH_4 (pmol g^{-1} d^{-1})**	
	Saturation	4° C	10° C
Direct	33	-120 ± 130	-710 ± 300
	66	-10 ± 10	-350 ± 50
	100	-130 ± 90	-450 ± 24
Isotope	33	-60 ± 60	-420 ± 20
	66	-10 ± 10	-240 ± 50
	100	-70 ± 40	-290 ± 150

Anaerobic 2.6 ppm CH_4	**70-80 cm**	
	CH_4 (pmol gfw^{-1} d^{-1})**	
	4° C	10° C
	-8.6±0.9 (-0.0005±0.0001)	-8.6±1.4 (-0.0006±0.00001)

Anaerobic 10 ppm CH_4	**70-80 cm**	
	CH_4 (pmol gfw^{-1} d^{-1})	
	4° C	10° C
	BDL	BDL

907

908 *Rates represent averages of 3 microcosms, except those marked by a *. Error shown is ±1 S.D.

909 ** Negative values represent oxidation of CH_4.

910 ***For the isotopic versus direct CH_4 oxidation measurements the 10°C CH_4 rates are calculated

911 from day 18 values. The 4°C CH_4 rates are calculated from 38 day values.

912

913 Table 3. ANOVA results examining microcosms testing water saturation, temperature, light/dark, and amendment effects on CO_2 and
914 CH_4 emissions.

		0-10 cm			30-40 cm			60-70 cm			70-80 cm		
		Water Saturation	Temperature	Interaction	Water Saturation	Temperature	Interaction	Water Saturation	Temperature	Interaction	Water Saturation	Temperature	Interaction
CO_2	F-ratio	2.26**	3.01	1.00	1.87	0.0004	6.73	23.53	1.79	19.52	6.56	0.18	0.01
	p-value	0.15	0.11	0.40	0.20	0.99	0.01*	0.0001*	0.21	0.0002*	0.01*	0.68	0.99
CH_4	F-ratio	29.22	41.63	19.49	17.07	123.21	23.57	1.02	72.03	0.70	0.21	3.42	1.15
	p-value	0.00002*	0.00003*	0.0002*	0.0003*	0.0000001*	0.00007*	0.39	0.000002*	0.51	0.81	0.09	0.35

		0-10 cm			PF (One-way ANOVA)
		Light/dark	Amendment	Interaction	Amendments
CO_2	F-ratio	16.94	2.87	2.93	1.28
	p-value	0.003*	0.10	0.10	0.39
CH_4	F-ratio	4.95	20.95	1.04	0.38
	p-value	0.06	0.0004*	0.4	0.77

915

916 * Statistically significant values are marked with a *.

917 ** All statistics show results from two-way ANOVA except for PF, which shows results from one-way ANOVA.

Table 4. The cellular oxidation rates normalized to CH_4 concentration from several studies.

CH_4 (ppmv)	T (°C)	Normalized Cellular Rate (fmol CH_4 $cell^{-1}$ day^{-1} ppmv-CH_4^{-1})
		This study
1.8	4	0.026
1.8	4	0.005
1.8	4	0.009
2.7	10	0.005
1.8	10	0.056
1.8	10	0.014
1.8	4	0.011
2.7	10	0.004
		Baani and Liesack, 2008
1000	25	0.10
700	25	0.09
600	25	0.08
100	25	0.07
10	25	0.02
1.75	25	0.02
		Knief and Dunfield, 2005
1000	25	0.11
1000	25	0.09
1000	25	0.03
1000	25	0.06
1000	25	0.08

1000	25	0.12
1000	25	0.02
1000	25	0.02
1000	25	0.02
1000	25	0.05
1000	25	0.01
100	25	0.06
100	25	0.05
100	25	0.01
100	25	0.07
100	25	0.05
100	25	0.03
10	25	0.04
10	25	0.01
10	25	0.05
10	25	0.05
10	25	0.04
1.75	25	0.02
1.75	25	0.02
1.75	25	0.02
1.75	25	0.03

		Girguis *et al.* 2003
5200	5	0.003
5200	5	0.002

		Liebner and Wagner, 2007
692	38	0.0007

591	28	0.0007
518	21	0.0010
424	12	0.0021
345	4	0.0044
305	0	0.0023

Table 5. Extrapolated field fluxes for CO_2 emission and atmospheric CH_4 uptake.

			CO_2 Rate (nmol g^{-1} d^{-1})		Flux mol CO_2 d^{-1}		CH_4 Rate (pmol g^{-1} d^{-1})		Flux µmol CH_4 d^{-1}	
Reference Rate	cm of depth	kg cryosol	4ºC 100% Sat	10ºC 33% Sat	4ºC 100% Sat	10ºC 33% Sat	4ºC 100% Sat	10ºC 33% Sat	4ºC 100% Sat	10ºC 33% Sat
0-10 cm	15	189	125.1 ± 13.5	98.2 ± 16.6	0.024±0.002*	0.019±0.003	34 ± 19	260 ± 60	-6.4±3.6*	-49.1±11.3
30-40 cm	30	486	16.1 ± 2.1	13.0 ± 2.9	0.008±0.001	0.006±0.001	7.5 ± 4.5	42.4 ± 2.7	-3.6±2.2	-20.6±1.3
60-70 cm	25	360	44.2 ± 2.2	36.5 ± 4.6	0.016±0.001	0.013±0.002	0.7 ± 1.0	7.3 ± 1.8	-0.3±0.4	-2.6±0.6
70-80 cm	10	144	33.5 ± 2.2	20.6 ± 4.6	0.005±0.0003	0.003±0.001	6.0 ± 0.4	1.6 ± 9.0	-0.9±0.1	-0.2±1.1
					Total mol CO_2 m^{-2} d^{-1}				Total µmol CH_4 m^{-2} d^{-1}	
					0.052±0.005	0.041±0.007			-11.2±6.2	-72.6±14.4

* Assuming a cryosol density of 1.8 g cm^{-3}, the total grams of cryosol comprising 1 m^{-2} was calculated down to a depth of 80 cm. This mass of cryosol was broken down into sections based on the 4 depths used for determining CO_2 production and CH_4 oxidation rates in the microcosms. Production and consumption was calculated for these 4 zones based on rates obtained from the two end member

925 conditions (4°C fully saturated and 10°C unsaturated) and then summed to give a scaled up estimate of total CO_2 emissions and total
926 CH_4 oxidation rates. CH_4 total flux assumes penetration of air with a CH_4 concentration above the methanotrophic threshold value.

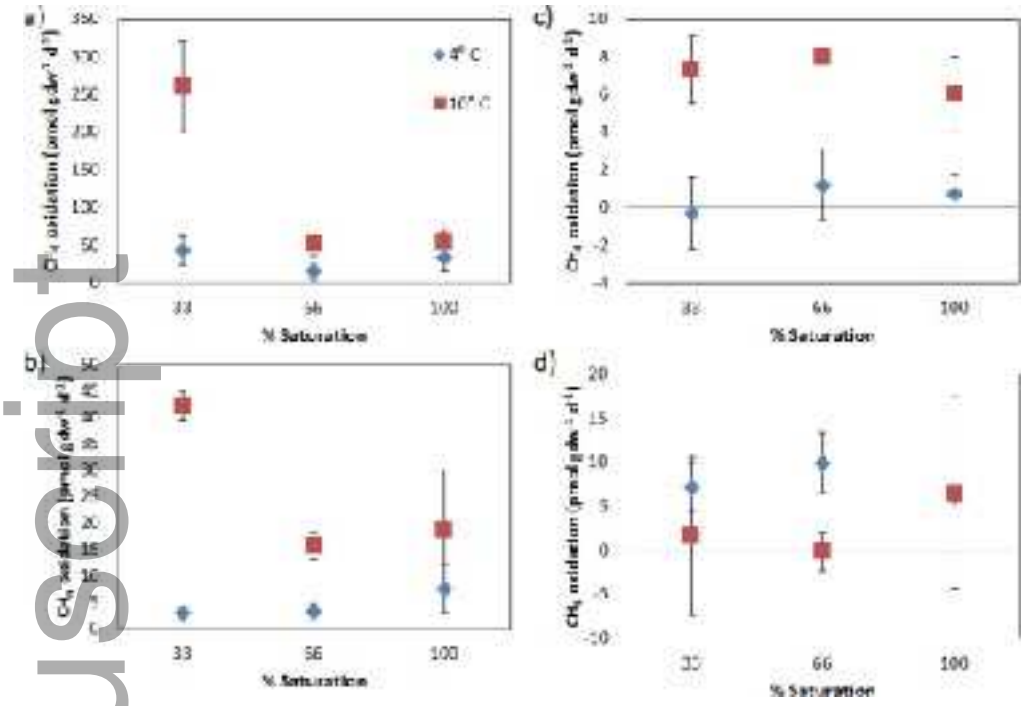

gbi_12193_f1.png

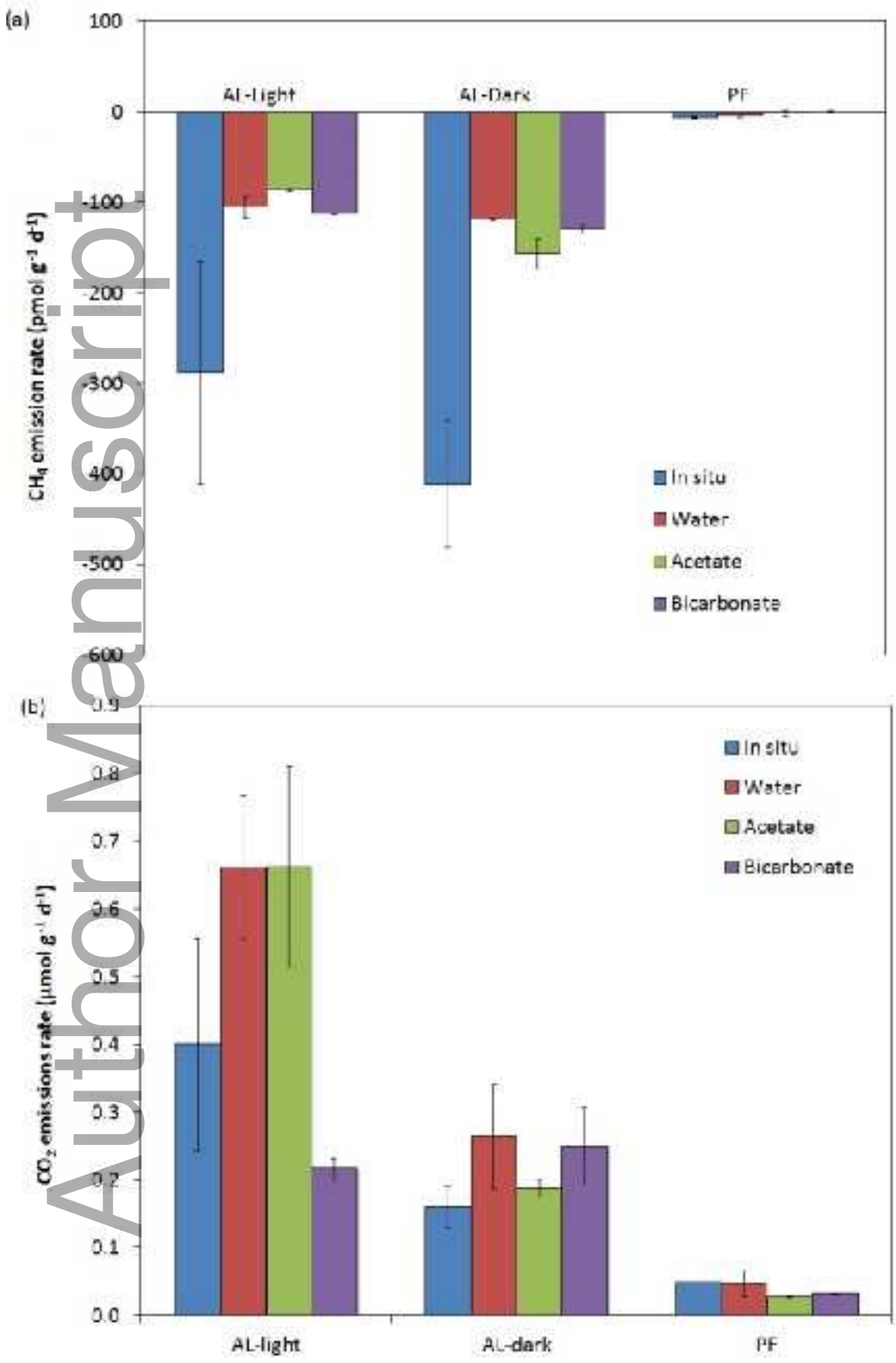

gbi_12193_f2.png

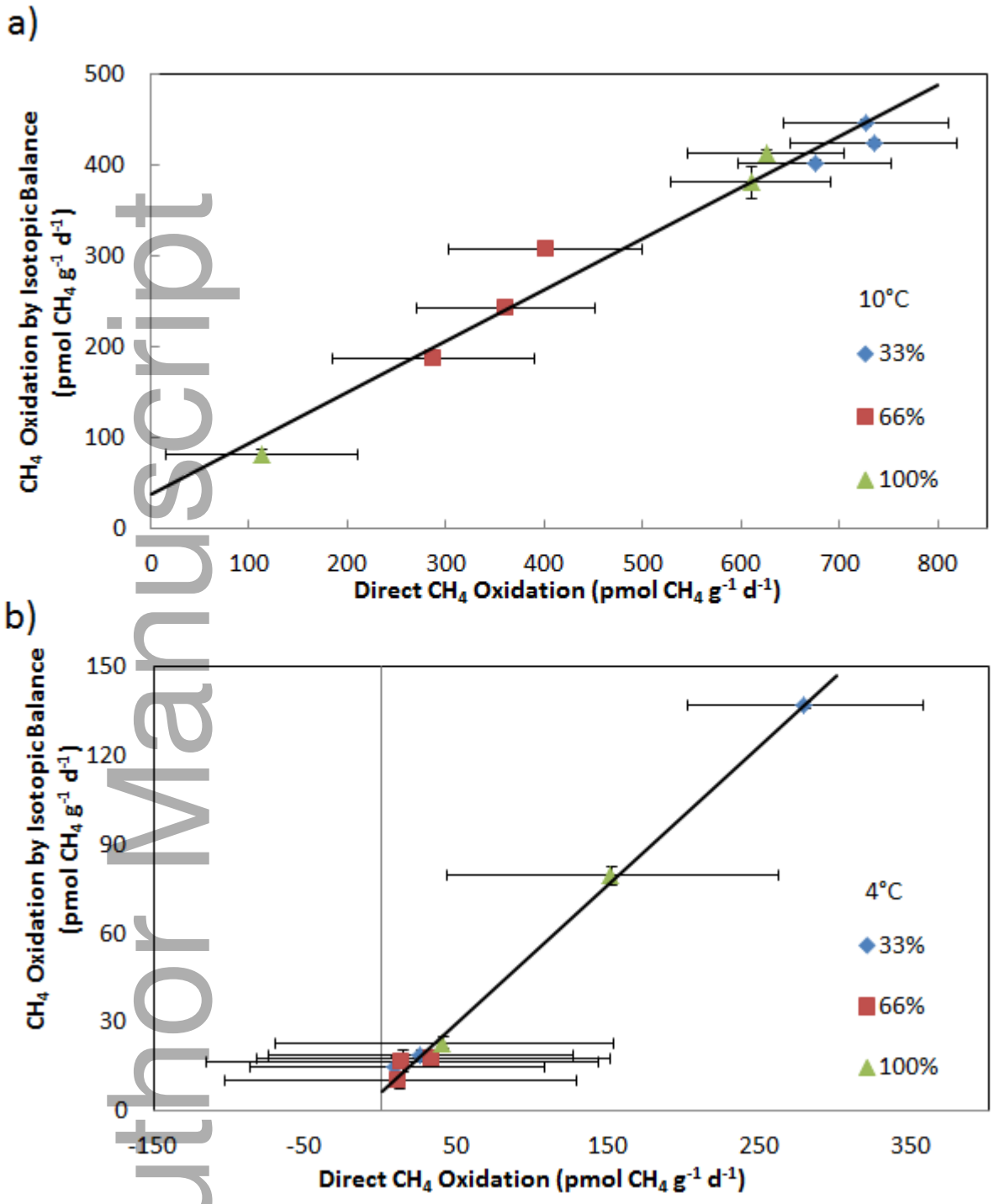

gbi_12193_f3.png

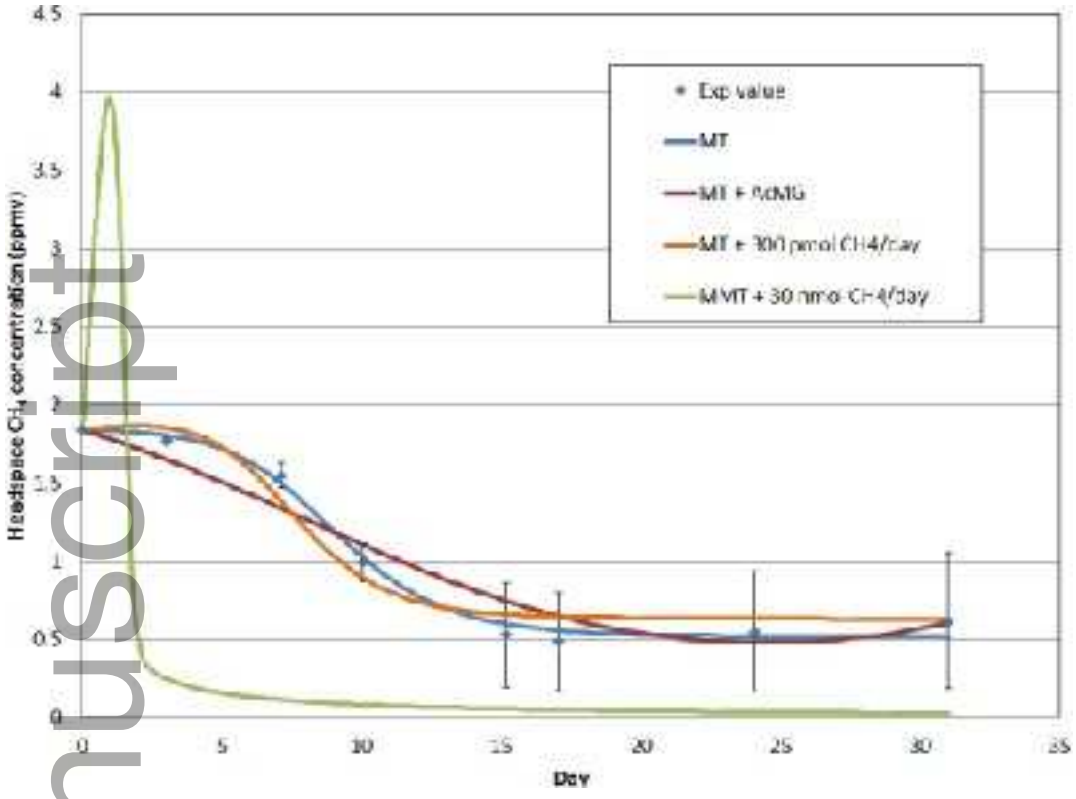

gbi_12193_f4.png

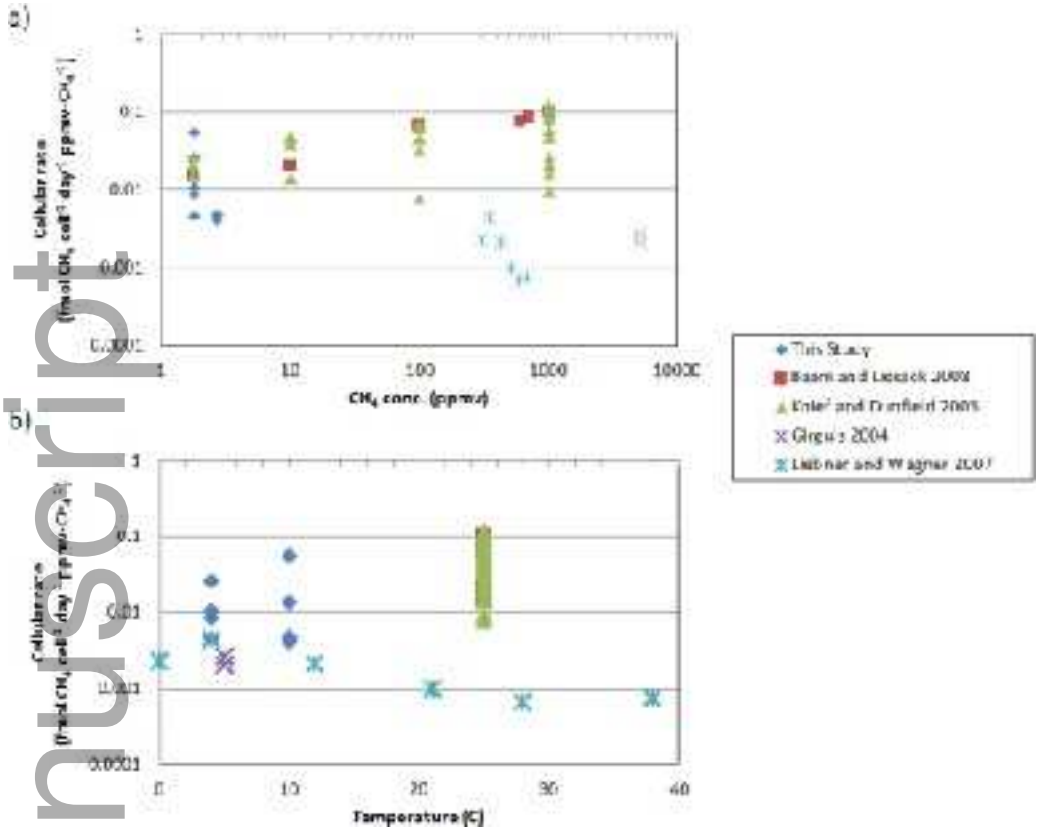

gbi_12193_f5.png